JACS
JOURNAL OF THE AMERICAN CHEMICAL SOCIETY
pubs.acs.org/JACS

Article

Dipolar Coupling as a Mechanism for Fine Control of Magnetic States in ErCOT-Alkyl Molecular Magnets

Maximilian G. Bernbeck, Angelica P. Orlova, Jeremy D. Hilgar, Milan Gembicky, Mykhaylo Ozerov, and Jeffrey D. Rinehart*

Cite This: J. Am. Chem. Soc. 2024, 146, 7243−7256

Read Online

ACCESS | Metrics & More | Article Recommendations | Supporting Information

ABSTRACT: The design of molecular magnets has progressed greatly by taking advantage of the ability to impart successive perturbations and control vibronic transitions in $4f^n$ systems through the careful manipulation of the crystal field. Herein, we control the orientation and rigidity of two dinuclear ErCOT-based molecular magnets: the inversion-symmetric bridged $[ErCOT(\mu\text{-}Me)(THF)]_2$ (**2**) and the nearly linear $Li[(ErCOT)_2(\mu\text{-}Me)_3]$ (**3**). The conserved anisotropy of the ErCOT synthetic unit facilitates the direction of the arrangement of its magnetic anisotropy for the purposes of generating controlled internal magnetic fields, improving control of the energetics and transition probabilities of the electronic angular momentum states with exchange biasing via dipolar coupling. This control is evidenced through the introduction of a second thermal barrier to relaxation operant at low temperatures that is twice as large in **3** as in **2**. This barrier acts to suppress through-barrier relaxation by protecting the ground state from interacting with stray local fields while operating at an energy scale an order of magnitude smaller than the crystal field term. These properties are highlighted when contrasted against the mononuclear structure $ErCOT(Bn)(THF)_2$ (**1**), in which quantum tunneling of the magnetization processes dominate, as demonstrated by magnetometry and ab initio computational methods. Furthermore, far-infrared magnetospectroscopy measurements reveal that the increased rigidity imparted by successive removal of solvent ligands when adding bridging methyl groups, along with the increased excited state purity, severely limits local spin−vibrational interactions that facilitate magnetic relaxation, manifesting as longer relaxation times in **3** relative to those in **2** as temperature is increased.

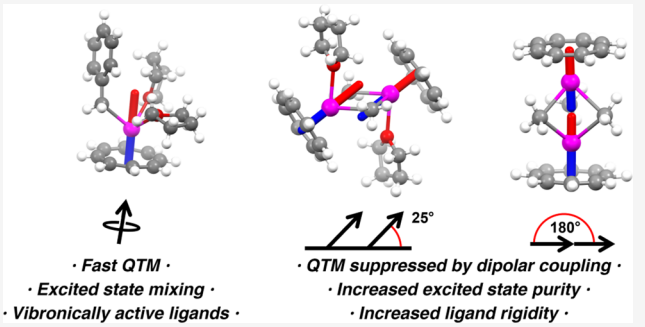

INTRODUCTION

The synthesis and study of electron spin materials at the molecular level, or molecular magnetism, is a synthetically driven approach to the daunting goal of bringing comprehensive structure−function design principles to atomic level magnetic interactions. Two milestones in this field, both arising from the analysis of a molecular metal oxide cluster Mn_{12},[1] were the characterization of an energy barrier to spin relaxation for a 0D system[2] and the manifestation of the resulting macroscopic quantum effect known as quantum tunneling of magnetization (QTM).[3−5] The study and control of QTM, in particular, have taken on a renewed significance with growing efforts to understand and design systems for initialization, evolution, and readout of quantum coherent and spin polarized states at the molecular level. Indeed, the promise of custom quantum spin interactions and molecular level magnet-like behavior has generated an entirely new and fruitful branch of molecular magnetism focused on discrete molecular systems known as single-molecule magnets (SMMs).[6−13]

Great strides have been made in the field of producing exceptional SMMs with individual spin centers, often denoted as single-ion magnets (SIMs) to denote their propensity to generate giant anisotropies through mechanisms inherent to the spin orbit interaction of an open shell ion with its local environment. Most often derived from transition metal or lanthanide centers, SIMs have generated drastic and continuous enhancement in mimicking bulk-magnet-like behaviors through careful design of their coordination environments.[14] Continued development has elucidated the importance of using highly symmetric ligand scaffolds[13,15−17] or synthetically controlling static[15,16,18−23] and dynamic[24−26] elements of the crystal field environment. Such design principles focus on two main parameters: the control of

Received: September 22, 2023
Revised: February 13, 2024
Accepted: February 14, 2024
Published: March 8, 2024

https://doi.org/10.1021/jacs.3c10412
J. Am. Chem. Soc. 2024, 146, 7243−7256

QTM, which is principally dependent on the probability of transitions between states of opposite moment, as determined by the degree of mixing, and thermal excitation via direct mechanisms, which depends on both the separation between magnetic states and the availability of vibrational modes coupled to these transitions.

While SIMs have pushed the boundaries of controlling spin−lattice relaxation out to technologically relevant temperatures, many quantum technologies require arrays of multiple coupled spins;[27−30] such coupling strategies work to enhance SMM relaxation behavior by affecting QTM at zero and applied fields as well.[31,32] Several examples exist of molecular systems with exceptional hysteretic behavior and an effective quenching of QTM by coupling highly anisotropic magnetic states, either directly or through a molecular bridge bearing spin density, to yield highly anisotropic "giant spins" akin to the clusters that established SMMs.[33−39] One route to building higher nuclearity molecular magnets is that of the "building block" approach, wherein several magnetic units with well-defined and synthetically robust ground states are linked to build systems with conserved anisotropy.[40−44] However, compatibility with open-shell bridges is difficult due to the charge-dense and highly penetrating radicals either destroying the anisotropy enforced by the comparatively weak crystal field or introducing large coupling so that magnetic energy levels become close and can easily mix.

One alternative is the exchange biasing imposed by neighboring spins − the dipolar interaction. This can be thought of as a local magnetic field perturbation generated by the anisotropic SIM dipole on its neighbors, effectively coupling populated magnetic states.[45−47] Dipolar coupling is well understood within condensed matter physics,[14,48−54] with both short- and long-range interactions described for macroscopic spin dynamics, magnetic domain formation, and phase transitions.[55−61] While such behavior has been noted in weakly coupled SMM clusters exhibiting relaxation behavior far slower than the local symmetry would seem to justify[62−69] and cited as a point of study in frustrated spin systems[70] and as a possible mechanism for entangling qubits,[30,71] it is more often in competition with other exchange mechanisms and serves to hinder desired properties.[66,72−74] Recently, we have proposed a perspective that such an interaction can instead behave as an advantageous extension of the current SMM design.[75] In the common heuristic of the 4f electronic structure involving successive perturbations (Figure 1), the dipolar interaction is a reliable method to provide the missing fine-tuning control of the wave function − weak enough to leave the crystal field approximation intact yet strong enough to generate well-defined restrictions on the wave function mixing that can almost completely reshape magnetic transitions in the quantum regime.[32,72]

Herein, we take advantage of the molecular anisotropic building unit ErCOT (COT = cyclooctatetraenide dianion, COT^{2-}), a coordinatively unsaturated 4f metal site with an isolated, robust M_J = 15/2 ground state and magnetic anisotropy that is well described by structural parameters.[75] A series of three alkyl-bound ErCOT complexes (Scheme 1 and Figure 2) highlights the degree of control that the dipolar interaction offers over coupling between isolated spin−orbit coupled states. A mononuclear species serves as a control, describing a system subject only to spin dynamics arising from its single-ion state structure and its interactions with the spin bath as a whole. By introduction of small, relatively rigid

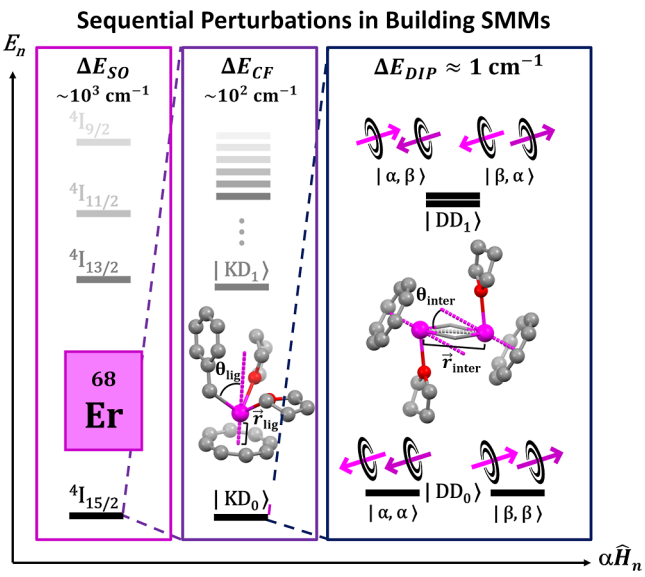

Figure 1. Illustrative progression of molecular magnetic perturbations. (Left) Spin−orbit coupling is principally governed by the choice in lanthanide. (Middle) Splitting of spin−orbit states into m_J levels is determined by the crystal field strength as enforced by the local ligand environment ($\vec{r}_{lig}$, θ_{lig}). (Right) Energy and moment of dipolar coupled states depend on the intermetal interactions as described by $\vec{r}_{inter}$ and θ_{inter}.

methyl ligands, two dinuclear species are isolated, clearly exhibiting ferromagnetic dipolar coupling that acts as a first-order perturbation upon the single-ion states. By deliberately directing the structurally pinned magnetic anisotropy axis at each center, we control the coupled energy landscape responsible for through-barrier relaxation processes operant at low temperatures, as supported by ab initio calculations and a combination of static and dynamic magnetometry. Such control illustrates the accessibility and pronounced results of manipulating this small internuclear perturbation while conserving the energy landscape provided by the crystal field. Furthermore, the introduction of rigid methyl groups displaces solvent ligands with high vibrational degrees of freedom and increases the symmetry in half of the coordination sphere of each metal. Using far-infrared magnetospectroscopy (FIRMS), we investigate the origin and efficiency of vibronic coupling responsible for the high-temperature relaxation processes of note.

RESULTS AND DISCUSSION

Synthesis and Structure. All reported complexes were synthesized using standard air- and water-free synthetic techniques (Section S1). Three complexes were isolated: one mononuclear complex $ErCOT(Bn)(THF)_2$ (**1**) and two dinuclear complexes: $[ErCOT(Me)(THF)]_2$ (**2**) and $Li[(ErCOT)_2(Me)_3]$ (**3**) (Bn = benzyl anion, $^-CH_2C_6H_5$; Me = methyl anion, $^-CH_3$; and THF = tetrahydrofuran) (Scheme 1). All were obtained through salt metathesis via the addition of an alkali metal salt of the appropriate anion to $ErCOT(I)(THF)_2$.

Solid-state molecular structures of all compounds were determined by single crystal X-ray diffraction with bulk purity supported by powder X-ray diffraction (Figure 2, Table 1, and Section S2) and a combination of NMR and Fourier transform infrared spectroscopy (Sections S3 and S4,

https://doi.org/10.1021/jacs.3c10412
J. Am. Chem. Soc. 2024, 146, 7243−7256

Scheme 1. Synthetic Overview for 1, 2, and 3

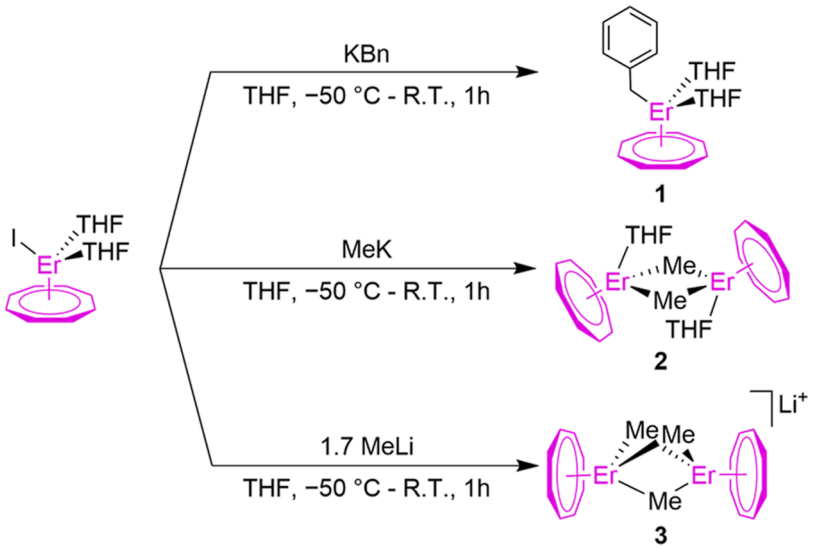

respectively). Metal−carbon bond lengths agree well with previously reported lanthanide alkyl structures.[76−93] Mononuclear **1** features the piano−stool geometry characteristic of the ErCOT moiety with the benzyl anion and THF ligands bound opposite to the COT^{2-} ring, giving an approximate C_s symmetry. Notably, the benzyl anion is monohaptic, as while the η^1 interaction is well-known,[76,83,88,90,94−105] lanthanide−benzyl complexes more commonly adopt an η^2 side-on interaction with the sp^2 hybridized $C-CH_2$ bond.[76,83,88,93,95,96,106−118] The orientation of the benzyl unit can be modified by changing the cosolvent, breaking this symmetry (Figure S4). However, only the structure featured in Figure 2 is further discussed herein. Complex **2** is an inversion symmetric combination of two pseudo-C_s symmetric units — a common dinuclear motif for LnCOT complexes.[119−130] Complex **3** has three identical bridging ligands and is most precisely C_s symmetric due to the incompatibility of the C_8 rotational axis of COT and the approximate C_3 axis between the three bridging methyl ligands. Both **2** and **3** have small internuclear distances [r_{Er-Er} = 3.5144(5) and 3.2393(9) Å, respectively], with **3** being the third shortest among discrete molecular erbium clusters after a methyl-bridged trinuclear cluster[131] and a pentadienyl-scaffolded dimer.[132] The $\vec{r}_{ErCOT}$ vectors in **2** are strictly parallel, as enforced by crystallographic symmetry, but they are oriented off-axis from the internuclear vector $\vec{r}_{int}$ by 22.90(7)°. In **3**, however, all three vectors are nearly colinear, deviating by only 0.4−2.3°. As previously demonstrated,[75] the relative strength of ErCOT dipolar interactions can be predicted by assuming that each SIM moment is pinned to its associated $\vec{r}_{ErCOT}$ vector and affecting a dipolar perturbation on the crystal field Hamiltonian. From this model, the parallel noncolinear arrangement (**2**) and parallel colinear arrangement (**3**) represent important contrasting experimental cases for understanding strongly anisotropic Ising coupling in the finite case.

Ab Initio Modeling. To model magnetostructural changes engineered into **2** and **3**, magnetic energy manifolds for the entire series **1**−**3** were predicted and evaluated with the SINGLE_ANISO and POLY_ANISO modules of OpenMolcas (Figure 3 and Table 2).[133] Typically, lanthanide-based SMMs can be modeled by using crystallographically determined atom coordinates as inputs without further geometry optimization. This has been found to be especially true where a particular metal−ligand pairing, such as the ErCOT unit, provides the majority of the stabilization energy. The addition of small, charge-dense ligands, however, can interfere with this effect by reducing the symmetry restrictions on spin state changes.[120] In the case of alkyl ligands, we can expect the orientation of the binding to be particularly influential as the orbitals carrying heavy 2p character impart strong locality and directionality on the electron density.[9,134−137] This electron density can then heavily impact the calculated magnetic anisotropy of the single ion states through increased state mixing, affecting both the predicted inter-Kramers dynamics and the expected coupling between them. While hydrogens were located from the crystallographic electron density map in **1** and **2**, the degree of disorder in **3** precluded meaningful assignment of methyl protons outside of an idealized geometry. As the calculated natural orbitals follow from input atom positions, optimized hydrogen positions were calculated with the ORCA computational package.[138,139] For the geometry optimization, open-shelled Er^{3+} was replaced with diamagnetic Y^{3+} due to its nearly identical ionic radius, and non-hydrogen atoms were frozen. Crystal packing is not explicitly considered in the gas-phase calculations, but by freezing the position of non-hydrogen atoms, the bulk of their effect on the conformation is assumed to be accounted for. Importantly, the optimized structure predicted significantly increased energy separations between Kramers doublets as well as decreased state mixing relative to the unoptimized structure. This optimized output was also more consistent with the experimental results and was therefore used in further descriptions of the energy landscape of **3**. Optimized geometries were also computed and used for magnetic calculations in **1** and **2**, and they were found to be largely consistent with the outputs obtained by using crystallographic positions. Thus, their experimentally determined structures were used.

For each complex, **1**−**3**, an isolated, crystal field split $J = \frac{15}{2}$ manifold was computed for each unique Er^{3+} center (Section S7.1). For mononuclear **1**, though manifolds for both crystal

https://doi.org/10.1021/jacs.3c10412
J. Am. Chem. Soc. 2024, 146, 7243−7256

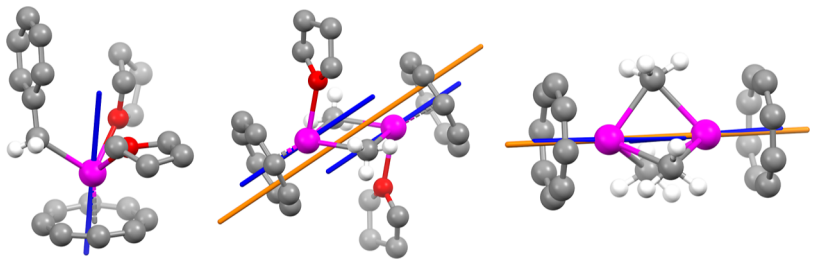

Figure 2. Crystallographically determined structures of **1** (left), **2** (middle), and **3** (right) with ab initio calculated ground-state single-ion (blue) and dipolar-coupled magnetic easy axes (orange). Nonalkyl hydrogens and outer-sphere cations are omitted for clarity. Alkyl hydrogens were located explicitly for **1** and **2**; hydrogens positions on bridging methyls in **3** were optimized in ORCA.

structures have been modeled, only the structure featured in Figure 2 is discussed here. For dinuclear complexes **2** and **3**, one metal center was replaced with diamagnetic Y^{3+} to limit the calculation to only one open-shell ion. All Er^{3+} centers displayed Kramers doublets ground states (KD_0) predominantly composed of the $M_J = \pm\frac{15}{2}$ eigenstate with principal magnetic axes lying nearly coincident with $\vec{r}_{ErCOT}$ (Figure 2). While there is minor variation in the composition of KD_0, the consequences of the alkyl coordination are more easily discerned in the first excited states (KD_1). These excited states lie within an energy regime typical of ErCOT complexes bound to charge-dense ligands.[120,140] The percentage of $M_J = \pm\frac{1}{2}$ character in the first excited states increases across the series, culminating in **3**, where it comprises nearly the entire excited state composition. Thus, even sans interatomic coupling, the first excitation in **3** represents a uniquely useful magnetic manifold for study: a coupling between the most axial Kramers configuration on the periodic table $\left|J = \frac{15}{2}, m_J = \pm\frac{15}{2}\right\rangle$ and the most rhombic one $\left|J = \frac{15}{2}, m_J = \pm\frac{1}{2}\right\rangle$ (Figure 3a). Here, thermal relaxation behavior is expected to be limited to transitions between relatively pure KD_0 and KD_1, whereas low-temperature relaxation behavior should be dictated by interactions within the lowest energy level at the energy of KD_0. Such a system presents a straightforward two-level system with a highly anisotropic ground state.

Both **2** and **3** bear closely spaced lanthanide ions with parallelly oriented highly anisotropic ground states. Magneto-

Table 1. Selected Distances and Angles for 1, 2, and 3

	1	2	3[a]
$\lvert\vec{r}_{Er-Er}\rvert$	N/A	3.5144(5) Å	3.2393(9) Å
$\lvert\vec{r}_{inter}\rvert_{min}$	8.3298 Å	7.3910(5) Å	7.3117(14) Å
$\boldsymbol{\theta}_{ErCOT-ErCOT}$	N/A	180.000(19)°	178.2(3)°
$\boldsymbol{\theta}_{ErCOT-ErEr}$	N/A	155.47(9)°	179.2(2)°

[a]Averaged.

structurally, this suggests a significant dipolar interaction. Thus, we consider the interactions between the ground states in **2** and **3** as modeled using the POLY_ANISO package in OpenMolcas (Figure 3b,c and Section S7.2).[141−143] To focus on the most important interactions, dipolar coupling was modeled only intramolecularly between single-ion states of KD_0 origin. Both **2** and **3** are predicted to exhibit a coupling of KD_0 states to give new ferromagnetically coupled dipole doublet ground states (DD_0) and antiferromagnetically coupled first excited states (DD_1), consistent with expectations for an end-to-end orientation of anisotropy axes. The calculated energy separation between these states is 2.055 cm^{-1} in **2** and 3.904 cm^{-1} in **3**, representing an increase by a factor of 1.90. The degree of control afforded by the dipolar interaction is immediately apparent. For example, the interaction is small compared to the energy gap between KD_0 and KD_1, allowing the coupled states to be treated as a first-order perturbation on the single-ion manifold while keeping the overall energy landscape intact. These separations are in good accordance with a simplified dipolar Ising model. When considering the $M_J = \pm\frac{15}{2}$ eigenstates to be purely axially anisotropic (g_z only), the dipolar interaction can be described with eq 1.

$$E_{dip} = \frac{\mu_0}{r^3}\left(\mu_1\cdot\mu_2 - 3\frac{(\mu_1\cdot\vec{r})(\mu_2\cdot\vec{r})}{r^2}\right) \quad (1)$$

Here, μ_1 and μ_2 are moments of individual magnetic centers, which in pseudospin-1/2 systems are $1/2\cdot g_z\cdot\mu_B$, and $\vec{r}$ represents the internuclear vector. When approximating g_z as coincident with $\vec{r}_{ErCOT}$, the coupled doublets are separated by $E_{dip} = 0.0078\cdot(g_z)^2$ cm^{-1} and $0.0128\cdot(g_z)^2$ cm^{-1} for **2** and **3**, respectively. Given the highly axial ground states of both **2** and **3**, g_z can be approximated to scale equally in both, and thus, the ratio of energies arising from a purely dipolar interaction ($E_{dip,3}/E_{dip,2}$) is predicted to be ∼1.6. This conforms to the trends observed in our calculated energy separation between DD_0 and DD_1 from POLY_ANISO calculations (*vide supra*) and with the fitting of the thermal dependence of ac magnetic susceptibility data (*vide infra*). Furthermore, the intermolecular distance (as measured by the closest Er−Er contacts) is over double the intramolecular distance between magnetic centers, suggesting an approximate 4- to 10-fold decrease in the strength of the dipole interaction between molecules relative to within them.

The foregoing discussion has developed a working model for the magnetic dipolar manifold that is relevant to the behavior governed by transition probabilities between the calculated eigenstates under a perturbing magnetic field.[144] The temperature and field dependence of the magnetic relaxation behavior for **1**−**3** is limited to, roughly, the energy separation between KD_0 and KD_1, which is still a useful parameter in **2** and **3** due to the relatively small perturbation imparted by dipolar coupling. This limit is set by the nature of the dipolar splitting, which in **2** and **3** further splits this manifold without increasing the overall energy scale. The dipolar interactions generate a highly directional perturbation that is large on the scale of random field fluctuations, making

https://doi.org/10.1021/jacs.3c10412
J. Am. Chem. Soc. 2024, 146, 7243−7256

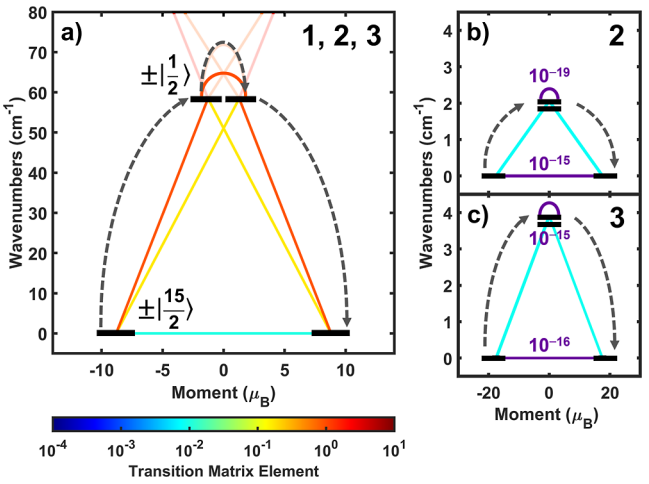

Figure 3. Predicted primary relaxation pathways, as described by SINGLE_ANISO and POLY_ANISO. (a) In the high-temperature regime, relaxation is predicted to occur primarily via excitation to the KD_1 manifold for **1**−**3**. In the low-temperature regime, only the KD_0 manifold is significantly populated, leading to QTM in **1**. (b,c) Low energy excitations in the coupled manifolds with DD_0 and DD_1 at the energy of KD_0 in **2** (b) and **3** (c) due to the exchange bias from dipolar coupling.

Table 2. Ab Initio Calculated Magnetic Parameters

	1	2	3[a]
ΔE, $KD_{0\rightarrow1}$	58.5 cm^{-1}	65.5 cm^{-1}	66(3) cm^{-1}
g_x, KD_0	0.011	0.006	0.007(6)
g_y, KD_0	0.052	0.026	0.03(2)
g_z, KD_0	17.610	17.559	17.502(2)
g_x, KD_1	0.106	12.453	11.6(2)
g_y, KD_1	1.317	6.077	7.2(2)
g_z, KD_1	14.595	1.241	1.15(4)
ΔE, $DD_{0\rightarrow1}$	N/A	2.055 cm^{-1}	3.904 cm^{-1}
g_x, DD_0	N/A	0.000	0.000
g_y, DD_0	N/A	0.000	0.000
g_z, DD_0	N/A	35.118	34.998
g_x, DD_1	N/A	0.000	0.000
g_y, DD_1	N/A	0.000	0.000
g_z, DD_1	N/A	0.000	0.705

[a]Structure is optimized and parameters are averaged over both centers.

it a highly effective limiter of random QTM mechanisms. These predictions are borne out in our calculations where over-barrier relaxation through the first excited state should be the favored relaxation pathway. At low temperatures, where the population of optical phonon modes with a sufficient energy to drive Orbach relaxation is dramatically decreased,[145] QTM should be rapid for **1**. However, in **2** and **3**, through-barrier transition probabilities within DD_0 and DD_1 drop to nearly zero compared to those of uncoupled KD_0. Meanwhile, thermally dependent excitations between DD_0 and DD_1 have approximately the same probability as that of the uncoupled QTM mechanism. The extremely slow QTM mechanism is effectively suppressed; therefore, transitions are limited to excitations between DD_0 and DD_1, which are predominantly controlled by the orientation of magnetic axes. The control of this new secondary barrier is then another useful tool toward tuning SMM behavior. More broadly, it can be thought of as a method for the rate control of spin population − a desirable trait for a much broader range of functionality. Furthermore, it represents the capacity of introducing a very small perturbation to dramatically affect relaxation by impacting the transition probabilities between the involved states. To probe the validity of these predictions, calculated properties were compared with physical measurements of spin-based observables.

Magnetometry Studies. Static and dynamic magnetic properties of **1**, **2**, and **3** were measured in a Quantum Design MPMS3 SQUID magnetometer to probe the effect of tuning the dipolar interactions (Section S5). First, temperature-dependent susceptibility measurements were performed to extract state information from the bulk response (Figure 4). The 300 K experimental $\chi_M T$ values measured under a

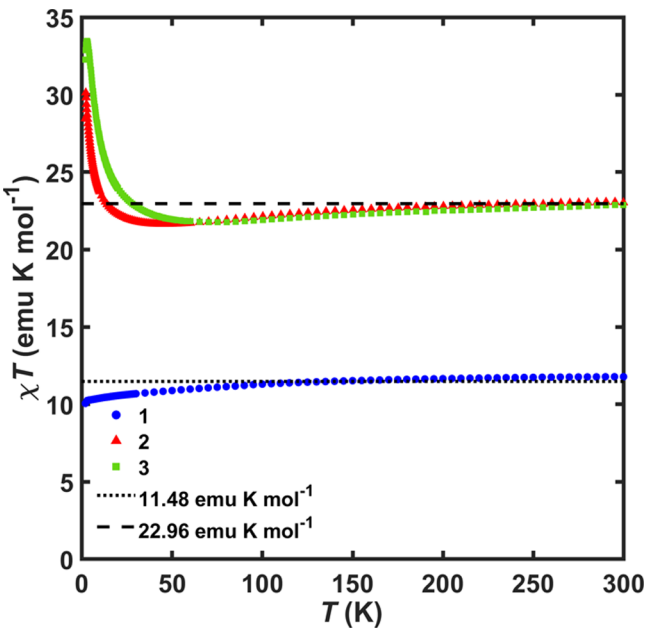

Figure 4. Temperature-dependent ZFC $\chi_M T$ measurements for **1** (blue circles), **2** (red triangles), and **3** (green squares) were collected at 1000 Oe. Dashed lines are plotted for theoretical $\chi_M T$ values of compounds with one and two Er^{3+} centers at 300 K.

1000 Oe applied field agree well with the theoretical values for the appropriate number of uncoupled Er^{3+} ions (11.78, 23.03, and 22.86 emu K mol^{-1} for **1**, **2**, and **3**, respectively; J = 15/2, g = 6/5 per ion; 11.48 emu K mol^{-1} per Er^{3+}).[146] At lower temperatures, $\chi_M T$ for **1** gradually decreases before decreasing more rapidly near 2 K, consistent with a typical depopulation of states in a SIM with low-lying excited states. For both **2** and **3**, $\chi_M T$ slightly decreases before rapidly increasing at lower temperatures, confirming the presence of ferromagnetic coupling. In **3**, this increase begins at higher temperatures and continues to a higher maximum value than in **2**, which coincides with the larger energy gap between DD_0 and DD_1 in **3**. This comparison holds under the assumption that the corresponding states have the same moment in both complexes, as corroborated by the output from POLY_ANISO.

Relaxation times (τ) were extracted from frequency-dependent AC susceptibility measurements by simultaneously fitting the in-phase (χ') and out-of-phase (χ'') components to a generalized Debye equation (Figure 5).[147] Cole−Cole plots of these fitted data form semicircles, and χ'' curves display

https://doi.org/10.1021/jacs.3c10412
J. Am. Chem. Soc. 2024, 146, 7243−7256

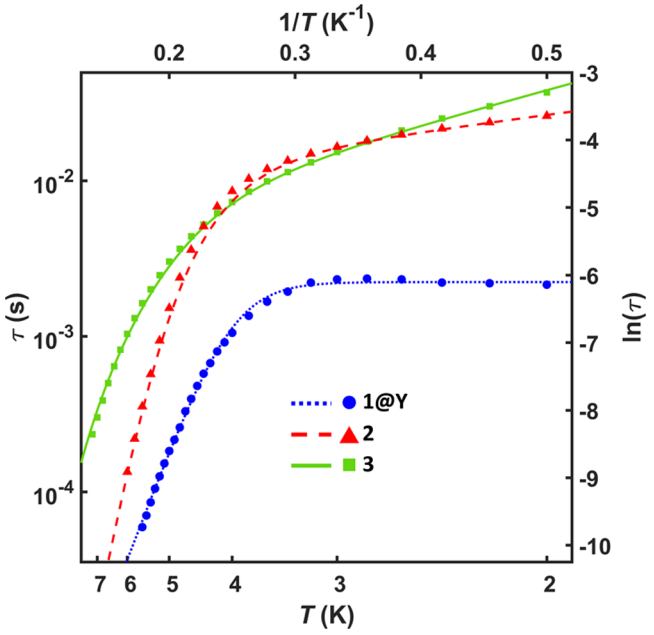

Figure 5. Relaxation behavior for **1@Y** (blue circles), **2** (red triangles), and **3** (green squares) as extracted from AC susceptibility versus frequency measurements. Extracted τ values are represented with points, and fits to eq 2 are plotted as curves of their respective colors.

one peak each. Thus, only a single relaxation time is described at each temperature for each compound. The τ values were fit to a combination of relaxation terms in eq 2

$$\tau^{-1} = \tau_0^{-1} e^{-U_{eff}/k_B T} + CT^n + \tau_{QTM}^{-1} + \tau_D^{-1} e^{-D_{eff}/k_B T} \quad (2)$$

with the first term representing an Orbach process, or a thermally activated pathway involving excited states, and the second term representing Raman, or vibronically coupled, processes. The third term accounts for QTM, whereas the fourth describes the thermal relaxation within the energy regime of KD_0 via excitation from the ferromagnetically coupled ground state (DD_0) to the antiferromagnetically coupled excited state (DD_1) over an energy barrier D_{eff}.[32,75] Both QTM and inter-DD thermal relaxations are expected to occur at very low temperatures, where sufficient thermal energy is not available for Orbach or Raman mechanisms to be comparatively efficient. QTM is expected to be prevalent in SIMs, and thermal relaxation through D_{eff} is expected to dominate when relaxation is influenced by highly axial interion coupling. In such a system, weak coupling introduces an energy barrier between the ferromagnetically and antiferromagnetically coupled states, and the suppression of QTM mechanisms limits relaxation to thermal excitations between them with long attempt times (τ_D) dictated by their enhanced anisotropies. Therefore, only one of either the third or fourth terms is included in fits to extracted τ values (Table 3).

Under zero applied field, only **2** and **3** display full peaks in χ'' vs ν within the measurable window of 0.1 to 1000 Hz. Curves for **1** display only stacked tails of peaks at frequencies above 1000 Hz. At 2 K, a fit to the incomplete curves places τ near 4.5×10^{-6} s (Figures S31 and S32 and Table S1). Such rapid relaxation is consistent with fast QTM mechanisms typical for SIMs—especially those with significantly mixed ground states. Dilution into an isostructural

Table 3. Fit Relaxation Parameters for 1@Y, 2, and 3

	1@Y	2	3
U_{eff}	34.3(7) cm^{-1}	66(3) cm^{-1}	79(6) cm^{-1}
τ_0	$1(2) \times 10^{-9}$ s	$2(2) \times 10^{-11}$ s	$2(7) \times 10^{-10}$ s
C		$1(5) \times 10^{-3}$	$3(2) \times 10^{-3}$
N		8.7(9)	6.9(2)
D_{eff}		1.6(3) cm^{-1}	3.5(1) cm^{-1}
τ_{QTM}/τ_D	$2.23(5) \times 10^{-3}$ s	$8(2) \times 10^{-3}$ s	$3.2(3) \times 10^{-3}$ s
τ_{max}	$2.35(14) \times 10^{-3}$ s	$2.61(6) \times 10^{-2}$ s	$3.7(1) \times 10^{-2}$ s

diamagnetic Y^{3+} lattice significantly reduces the effect of transient fields caused by nearest-neighbor intermolecular interactions. Thus, a 95:5 mol equivalent Y/Er mixture of **1** (**1@Y**) was prepared, and full peaks were observable in χ'', allowing the extraction of relaxation times below 6 K. Though fast relaxation processes facilitated by nearest-neighbor interactions are suppressed upon dilution, the fast QTM associated with uncoupled magnetic centers persists.

Both **2** and **3** show SMM behavior below 6 and 7 K, respectively, without dilution. When plotting ln (τ) vs $1/T$, both complexes show Arrhenius behavior at their highest temperatures, followed by an attenuation of the temperature dependence of relaxation, culminating in a very weakly temperature-dependent region near 2 K. Notably, neither complex displays a temperature-independent region consistent with QTM being the dominant process. All fit parameters are consistent with ab initio calculations, and the D_{eff} for **3** is expectedly larger than that for **2**. Some notable features when comparing the evolution of τ can be explained using D_{eff} and τ_D. Notably, **3** has a slightly larger barrier U_{eff} and τ_0 than **2**, and D_{eff} is approximately twice as large. However, τ_D is faster in **3** than in **2**, and thus, there is an intermediate region wherein **2** relaxes more slowly than **3**. Fit parameters for **2** and **3** were corroborated by measurements under a small applied field of 800 Oe as well as for diluted samples (Section S5). Under an applied field, the D_{eff} and τ_D remain largely consistent for both **2** and **3**. Diluted samples **2@Y** and **3@Y** were prepared by cocrystallization of pre-prepared Er^{3+} and Y^{3+} samples of **2** and **3**. In both diluted samples, the presence of ferromagnetic coupling is still observed, though metal scrambling is apparent by the much broader peaks in χ'' vs ν resembling two separate overlapping mechanisms. A much higher degree of metal scrambling is noted for **3@Y** than in **2@Y**, as evidenced by the relative attenuation of the low-temperature increase in $\chi_M T$ values. This is a common problem when diluting polynuclear structures;[73] we attribute this in our systems to the ability to crystallize **2** at subzero temperatures, but the room-temperature conditions required for **3** can allow for more lability in solution. Regardless, relaxation parameters for **2@Y** agree well with the undiluted complex, and while the apparent onset of QTM in **3@Y** complicates interpretation, relaxation behavior at low temperatures is still thermally dependent and no attenuation of high-temperature relaxation is observed.

The relaxation of **1** can be juxtaposed against that of **2** and **3** to illustrate the degree of control afforded by dipolar coupling and the resulting consequences for magnetic properties. Primarily, the uncoupled, comparatively weaker moment of **1** is highly susceptible to the complex, low symmetry dipolar environment, which acts to enhance the available QTM processes within individual ions. This same

https://doi.org/10.1021/jacs.3c10412
J. Am. Chem. Soc. 2024, 146, 7243−7256

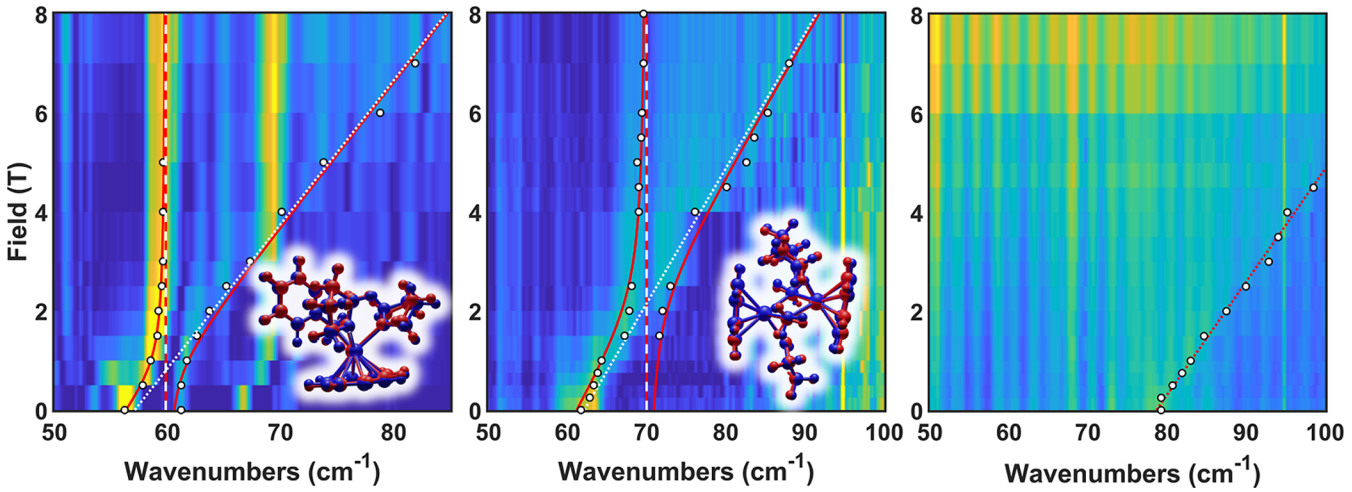

Figure 6. Lowest energy transitions visible in FIRMS spectra for **1** (left), **2** (middle), and **3** (right). White dots represent experimental points, orange curves show full fits as described in the main text and Supporting Information, and dashed and dotted lines represent uncoupled vibrational modes and magnetic transitions extracted from FIRMS data, respectively.

sensitivity to QTM and neighboring spins is not present in **2** or **3**. Following the predictions afforded by POLY_ANISO, low-temperature relaxation in these complexes is dominated by the small thermal barrier imparted by intramolecular dipolar coupling, which is directed to enhance the local anisotropy. The probability of QTM is consequently lowered by over 10 orders of magnitude in the case of specific levels determined by the orientation of the anisotropy vector. Importantly, this mechanism is not a result of achieving a well-isolated coupling state, but instead, it is more akin to a targeted exchange bias of the states responsible for magnetic relaxation. While the dipole−dipole interaction between the two ions is weak, it is important to note that it is far larger than the intermolecular dipolar fields between neighboring molecules, making both **2** and **3** relatively inert to fluctuations caused by their nearest neighbors. This is made clear by the lack of significant change in the relaxation dynamics of **2@Y**, and in **3@Y**, the partial removal of intramolecular coupling seems to hasten relaxation. An alternative interpretation of this result, as might be garnered from the crystal structure of **3**, is the removal of a high symmetry bulk dipolar field arising from intermolecular interactions that enhances relaxation.[148] In the absence of further supporting data, we do not explore this beyond speculation, but the possibility invites future investigations of crystal engineering with coupled systems.

Far-Infrared Magnetospectroscopy. To complement the description of the local magnetic landscape that we have crafted, FIRMS was employed to probe vibronically coupled magnetic transitions. While this technique is most often employed in surveying extended magnetic solids and qubit candidates,[26,29,149−154] recent work has employed FIRMS alongside single-crystal Raman magnetospectroscopy and inelastic neutron scattering experiments to probe zero-field splitting parameters in transition metal complexes[155,156] and Kramers doublet separations in lanthanide SMMs[25,157,158] with energy separations too large to feasibly be observed in electron paramagnetic resonance (>∼ 100 cm^{-1}) or that do not fulfill the necessary selection rules ($\Delta M_J = \pm 1$). While magnetic transitions are often IR-allowed, either by following magnetic/electric dipole selection rules or by relaxing these rules via 4f-5d orbital mixing, these transitions are very weak compared to molecular vibrational and phonon modes.[159] The high difference in moments makes the overlap induced by electromagnetic radiation far poorer for these transitions than for pure vibronic transitions. Magnetic transitions can, however, be isolated from transmission spectra by using the field dependence of the magnetic moment to remove vibrational modes uncoupled from magnetic transitions. The resulting heat map then shows the intensity and energy of a transition as a function of the applied magnetic field. While these spectra cannot be easily deconvoluted into crystal lattice vibration modes (phonons) and local molecular vibrational modes, tentative assignments of these transitions can be made to local vibrations modeled by density functional theory (DFT) calculations performed on optimized structures. Here, Er^{3+} was replaced with the closed-shell Lu^{3+} ion rather than Y^{3+} due to its more similar electronic structure and nuclear mass for calculating vibrational energies, and the entire structure's geometry was optimized. Due to the density of vibrational modes within this region and the limitations of modeling lanthanide complexes with DFT, these assignments are not meant to pinpoint the atomic origins but rather to suggest the type of mode within the correct energy range to facilitate a dynamic coupling.

FIRMS measurements at 4.5 K were performed from 0 to 17 T for **1**, **2**, and **3** (Figure 6 and Section S8). Weak, magnetically dependent peaks are visible between 30 and 700 cm^{-1} for all three to varying degrees, as discussed below. All transitions' intensities dramatically increase when in close energy proximity to a coupled vibrational mode, maximizing when the two are resonant. On approach, the magnetic and vibration transitions mix in an observable avoided crossing. Since only states involving KD_0 are expected to be meaningfully populated for all three species at 4.5 K, the magnetic transitions are all assumed to be excitations from KD_0 (or the relevant dipolar splitting manifold for **2** and **3**). The high fields used in FIRMS experiments dictate that the Zeeman interaction is now a larger perturbation than the dipolar interaction by an order of magnitude, leading to an energy landscape described by a simplified phenomenological spin−phonon coupling Hamiltonian at the resolution of the crystal field of the individual single-ion spin centers, as described by SINGLE_ANISO (described in Section S9).

https://doi.org/10.1021/jacs.3c10412
J. Am. Chem. Soc. 2024, 146, 7243−7256

Since relaxation is predominantly measured to occur within KD_0 and KD_1, we focus on transitions below 100 cm^{-1}. As KD_0 and KD_1 are relatively close together in all three complexes, mixing between them is expected in the high fields in the experiment. Furthermore, the Zeeman perturbation energy in high fields quickly becomes larger than that of dipolar coupling. Thus, for simplicity, magneto-vibronic transitions can be described in terms of single-ion states. Within the low energy landscape, two separate instances of one magnetic transition coupled to one vibrational mode were observed for **1**, a single magnetic transition coupled to one vibrational mode was observed for **2**, and only an exceedingly weak magnetically dependent transition without any resolvable coupled vibrational modes was discernible for **3**. The lowest transition for **1** appears at 57(1) cm^{-1}, consistent with our calculated and experimentally observed barriers. Assuming that the transition originates from the $M_J = +\frac{15}{2}$ state, this is also consistent with a transition to the $M_J = +\frac{1}{2}$ state (moments $\mu_{KD1,fit} = -1.4(8)\ \mu_B$, and $\mu_{KD1,calc} = \pm 1.3\ \mu_B$). The coupled vibrational mode at 59.8(1) cm^{-1} most closely resembles a computed librational mode at 60.9 cm^{-1} where twisting modes of the THF ligands and rocking of the COT^{2-} dominate. A second transition is visible in the same region at 67(2) cm^{-1} coupled to a vibrational mode at 69.7(3) cm^{-1}. The excited state moment is $\mu_{KD,fit} = -0.3(27)\ \mu_B$ under the assumption that the same $M_J = +\frac{15}{2}$ state is the origin of the transition. While said magnetic transition has a higher energy than predicted for either isolated structure, the similarity both in the coupling strength (spin−phonon coupling constant $\Lambda_1 = 1.6(4)$ cm^{-1} and $\Lambda_2 = 1.4(6)$ cm^{-1}) and in the difference in the moment between states implies some congruence between the two transitions.

The fit magnetic transition for **2** at 62(1) cm^{-1} also corresponds well to the ab initio value of 65.5 cm^{-1}. The moment of KD_1 is similarly consistent [$\mu_{fit} = -0.9(9)\ \mu_B$ and $\mu_{calc} = \pm 0.93\ \mu_B$]. As in **1**, the corresponding DFT calculated vibrational mode at 72.1 cm^{-1} describes libration involving both THF ligands with moderate twisting and wagging motions, and the transition is coupled more strongly at $\Lambda_1 = 2.9(4)$ cm^{-1}. Interestingly, only one of the two COT ligands has a large displacement in its "rocking mode" within the libration. Lastly, the bridging methyl ligands twist about the axis connecting both ligands' atoms.

The lowest magnetically coupled vibrational mode in **3** displays far weaker intensity than those in both **1** and **2**. However, a weak absorption linearly dependent with the field can be resolved. In stark contrast to the other two complexes, the lowest magnetic transition visible in FIRMS for **3** does not appear to couple to any nearby vibrational modes. There is a slight increase in intensity below 1 T near 80 cm^{-1} and above 4 T near 100 cm^{-1}, but the weak signal-to-noise ratio and experimental artifacts preclude meaningful discussion of vibronic coupling in these regions. The weak linearly magnetically dependent transition can be fit to a simple Zeeman perturbation

$$\Delta_{KD} + B\mu_B(\Delta\mu_{KD}) = \Delta_{obs} \quad (3)$$

to extract Δ_{KD} and $\Delta\mu_{KD}$. Here, Δ_{KD} is 78.6(6) cm^{-1}, and the transition corresponds to an excitation to a state with a moment of $-0.6(3)\ \mu_B$. The fit barrier is higher than calculated, matching most closely to the first excited state ($\Delta_{1,calc} = 66.3$ cm^{-1}), but corresponds well to that measured via magnetometry ($U_{eff} = 79(6)$ cm^{-1}). The moment of the excited state likewise resembles that of the first excited state ($\mu_{KD} = \pm 0.56\ \mu_B$). The closest vibrational modes calculated by DFT lie at 68.29 and 69.69 cm^{-1}, corresponding to twisting modes of the bridging methyl ligands and slight rocking of the COT rings, respectively. Above the range in which the first transition is resolvable, the first available mode to couple to is at 108.03 cm^{-1}, which corresponds almost exclusively to twisting motions in the methyl ligands.

While the assignment of local molecular vibrational modes as mediators of the spin−lattice interaction is qualitative, it allows for testable hypotheses regarding molecular design. Specifically, both **1** and **2** display significant motion within the THF ligands. Considering both the large degree of freedom in movement within the ligand and the electron density of the coordinated oxygen atom, such a motion should perturb magnetic states so as to allow for thermally assisted QTM. Decreasing the number of coordinated THF ligands per Er^{3+} center from two in **1** to one in **2** appears to suppress this based on the decreased absorption intensity. Thus, more rigid ligands or, in the case of **3**, a total lack of hard Lewis basic solvent ligands may suppress coupling, as has been noted in other discussions.[17,160] The other major contributor to motion—the rocking of the COT^{2-} ligand—cannot be so easily suppressed. However, introducing bulky substituents, such as the silyl groups that have achieved much synthetic success,[11,75,129,161,162] could limit the degree of motion available to the scaffold. However, caution must also be taken not to introduce additional entropic vibrational modes within the added functional groups. Additionally, while the increased pseudosymmetry in **3** limits the number of IR active modes, the possibility of Raman-active modes prevents us from drawing clear conclusions relating to it.

While intense magnetic transitions can be seen in the FIRMS heatmaps of all three compounds, the lowest energy transitions show a dramatic difference in the change of their intensities; this merits additional discussion. Alongside the control of internal modes of vibrational degrees of freedom, the spectra we included herein can illustrate the effect of tuning the magnetic state composition as a result of the crystal field. Selection rules dictating intramanifold transitions are not well established, though past discussions have pointed to transitions being magnetic dipole and electric dipole allowed. Such rules dictate that a transition between pure M_J states should be allowed for $\Delta M_J = \pm 1$, though this can be relaxed through mixing. Such a case is observed when juxtaposing the heat maps of **1** and **2** against that of **3** in the context of the state composition of their Kramers doublets as modeled by SINGLE-ANISO. The heatmap in **1** reveals a relatively intense magnetically dependent transition in the lowest energy excitation. The corresponding transition in **2** is noticeably weaker, and in **3**, the magnetically dependent peaks in the lowest transition are barely resolvable. Such a progression corresponds well to the purity of the first manifold of excited states composed of interactions involving KD_1. While single-ion calculations for **1**−**3** reveal KD_0 manifolds of almost pure $M_J = \pm\frac{15}{2}$ and KD_1 principally composed of $M_J = \pm\frac{1}{2}$, the degree of mixing of the $M_J = \pm\frac{13}{2}$ into KD_1 decreases markedly from **1** to **3**. In **1**, it comprises 13% of KD_1, whereas in **2**, it drops to 2%, and in **3**, it is less

https://doi.org/10.1021/jacs.3c10412
J. Am. Chem. Soc. 2024, 146, 7243−7256

than 1%. Meanwhile, the composition of $M_J = \pm\frac{1}{2}$, to which a transition from $M_J = \pm\frac{15}{2}$ would be least allowed, increases from 54 to 81 and 92% in **1**, **2**, and **3**, respectively. This trend is also reflected in the ab initio derived transition probabilities between KD_0 and KD_1, which are nearly an order of magnitude smaller in **2** and **3** than those in **1**.

CONCLUSIONS

We have presented alkyl-bridged dinuclear SMMs that utilize the placement of internal fields to direct dipolar coupling as an alternative to orbital exchange as a means of fine control over the spin manifold. The dramatic increase in relaxation times at all temperatures observed in the closely bound dinuclear complexes **2** and **3** relative to that in the mononuclear **1** demonstrates how the precision of molecular synthesis offers the chance to transform the oft invoked concept of exchange bias into a design principle for quantum spin architectures. Whereas strong orbital exchange can be used to isolate large spin states, it can also forfeit much of the precise spatial anisotropy garnered by tuning the single-ion crystal field. The use of directed dipolar interactions preserves the overall anisotropy and moment generated by the dominant crystal field interaction while protecting states against random field fluctuation-induced QTM mechanisms. A clear manifestation of this is seen in how the collinear, high pseudosymmetry anisotropy axes of **3** result in exceptional changes in the relaxation dynamics within a temperature regime of nearly equivalent Boltzmann distribution across the manifold of coupled states. Additionally, through the FIRMS technique, the low energy spectrum is monitored to study how the changes in structural rigidity, and selection rules imparted by **1**−**3** yield very different mixing between the spin and lattice components. Absorptions akin to the magnetic relaxation pathway decrease in intensity across the series in **1**−**3**, with computational results indicating that both the removal of the highly entropic THF ligands and the increased purity of the excited $M_J = \pm\frac{1}{2}$ state are likely to play a role.

In summary, **1**−**3** have been studied comparatively to determine the effects of high-moment, high-anisotropy ions to direct internal dipolar fields and generate a model that describes relaxation behavior in the long time scale regime where it is controlled by the ground single-ion state. Within this regime, relaxation is highly susceptible to random fluctuation factors, unless there are specifically engineered control principles geared to this scale. The results from **1**−**3** suggest that construction of larger scale architectures assisted by modeling of spin relaxation through Ising-type models offer a natural direction of expansion for single-ion design to higher nuclearities in lanthanide molecular magnetism: it preserves the crystal field design principles carefully crafted over the past decade through the introduction of a much smaller perturbation while allowing for the addition of new ions with a known spin structure based on an additional spin bias (internal Zeeman) Hamiltonian term. As a future direction, it affords an additional mode of observation, modeling, and control with responses to magnetic, crystalline, and electromagnetic fields.

ASSOCIATED CONTENT

Supporting Information

The Supporting Information is available free of charge at https://pubs.acs.org/doi/10.1021/jacs.3c10412.

Detailed synthetic procedures, crystallographic parameters and characterization, bulk spectroscopic characterization, experimental magnetic data, computational setup and salient output, FIRMS measurements, and description and derivation of magnetovibronic coupling fitting equations (PDF)

Representation of salient vibrational modes in **2** included as animation (GIF)

Representation of salient vibrational modes in **1** included as animation (GIF)

Accession Codes

CCDC 2282642−2282650 contain the supplementary crystallographic data for this paper. These data can be obtained free of charge via www.ccdc.cam.ac.uk/data_request/cif, or by emailing data_request@ccdc.cam.ac.uk, or by contacting The Cambridge Crystallographic Data Centre, 12 Union Road, Cambridge CB2 1EZ, UK; fax: +44 1223 336033.

AUTHOR INFORMATION

Corresponding Author

Jeffrey D. Rinehart − *Department of Chemistry and Biochemistry, University of California—San Diego, La Jolla, California 92093, United States;* orcid.org/0000-0002-5478-1995; Email: jrinehart@ucsd.edu

Authors

Maximilian G. Bernbeck − *Department of Chemistry and Biochemistry, University of California—San Diego, La Jolla, California 92093, United States;* orcid.org/0000-0001-6329-5860

Angelica P. Orlova − *Department of Chemistry and Biochemistry, University of California—San Diego, La Jolla, California 92093, United States;* orcid.org/0000-0002-2446-1384

Jeremy D. Hilgar − *Department of Chemistry and Biochemistry, University of California—San Diego, La Jolla, California 92093, United States;* orcid.org/0000-0001-5142-3079

Milan Gembicky − *Department of Chemistry and Biochemistry, University of California—San Diego, La Jolla, California 92093, United States;* orcid.org/0000-0002-3898-1612

Mykhaylo Ozerov − *National High Magnetic Field Laboratory, Tallahassee, Florida 32310, United States;* orcid.org/0000-0002-5470-1158

Complete contact information is available at: https://pubs.acs.org/10.1021/jacs.3c10412

Funding

This research was funded through the National Science Foundation Division of Chemistry #2024650. The National High Magnetic Field Laboratory is supported by the National Science Foundation through NSF/DMR-1644779 and the State of Florida.

Notes

The authors declare no competing financial interest.

■ ACKNOWLEDGMENTS

The authors would like to thank the UCSD Crystallography facility for their facilities and expertise, the W. M. Keck Laboratory for Integrated Biology for use of their computational cluster workstation, and the Figueroa Group for the use of their diamond anvil FT-IR instrument. A portion of this work was performed at the National High Magnetic Field Laboratory. We also wish to thank Drs. John Lopp and Joseph Palasz for their valuable discussion regarding the ORCA computational package and DFT calculations.

■ ABBREVIATIONS

SMM, single-molecule magnet; QTM, quantum tunneling of the magnetization; COT, cyclooctatetraene dianion; THF, tetrahydrofuran; DME, dimethoxyethane; SIM, single-ion magnet

■ REFERENCES

(1) Lis, T. Preparation, Structure, and Magnetic Properties of a Dodecanuclear Mixed-Valence Manganese Carboxylate. *Acta Crysallogr. Sect. B* **1980**, *36* (9), 2042−2046.
(2) Sessoli, R.; Gatteschi, D.; Caneschi, A.; Novak, M. A. Magnetic Bistability in a Metal-Ion Cluster. *Nature* **1993**, *365* (6442), 141−143.
(3) Caneschi, A.; Gatteschi, D.; Sessoli, R.; Barra, A. L.; Brunel, L. C.; Guillot, M. Alternating Current Susceptibility, High Field Magnetization, and Millimeter Band EPR Evidence for a Ground S = 10 State in [Mn12O12(Ch3COO)16(H2O)-4].2CH3COOH.4H2O. *J. Am. Chem. Soc.* **1991**, *113* (15), 5873−5874.
(4) Sessoli, R.; Tsai, H. L.; Schake, A. R.; Wang, S.; Vincent, J. B.; Folting, K.; Gatteschi, D.; Christou, G.; Hendrickson, D. N. High-Spin Molecules: [Mn12O12(O2CR)16(H2O)4]. *J. Am. Chem. Soc.* **1993**, *115* (5), 1804−1816.
(5) Thomas, L.; Lionti, F.; Ballou, R.; Gatteschi, D.; Sessoli, R.; Barbara, B. Macroscopic Quantum Tunnelling of Magnetization in a Single Crystal of Nanomagnets. *Nature* **1996**, *383* (6596), 145−147.
(6) Sorace, L.; Benelli, C.; Gatteschi, D. Lanthanides in Molecular Magnetism: Old Tools in a New Field. *Chem. Soc. Rev.* **2011**, *40* (6), 3092−3104.
(7) Habib, F.; Murugesu, M. Lessons Learned from Dinuclear Lanthanide Nano-Magnets. *Chem. Soc. Rev.* **2013**, *42* (8), 3278−3288.
(8) Liddle, S. T.; van Slageren, J. Improving F-Element Single Molecule Magnets. *Chem. Soc. Rev.* **2015**, *44* (19), 6655−6669.
(9) McInnes, E. J. L. Introduction to Molecular Magnetism. From Transition Metals to Lanthanides By Cristiano Benelli and Dante Gatteschi. *Angew. Chem., Int. Ed.* **2016**, *55* (6), 1959.
(10) Edelmann, F. T. Lanthanides and Actinides: Annual Survey of Their Organometallic Chemistry Covering the Year 2017. *Coord. Chem. Rev.* **2018**, *370*, 129−223.
(11) Liu, J.-L.; Chen, Y.-C.; Tong, M.-L. Symmetry Strategies for High Performance Lanthanide-Based Single-Molecule Magnets. *Chem. Soc. Rev.* **2018**, *47* (7), 2431−2453.
(12) Guo, F.-S.; Bar, A. K.; Layfield, R. A. Main Group Chemistry at the Interface with Molecular Magnetism. *Chem. Rev.* **2019**, *119* (14), 8479−8505.
(13) Goodwin, C. A. P. Blocking like It's Hot: A Synthetic Chemists' Path to High-Temperature Lanthanide Single Molecule Magnets. *Dalton Trans.* **2020**, *49*, 14320−14337.
(14) Wernsdorfer, W. Quantum Dynamics in Molecular Nanomagnets. *C. R. Chim.* **2008**, *11* (10), 1086−1109.
(15) Gupta, S. K.; Murugavel, R. Enriching Lanthanide Single-Ion Magnetism through Symmetry and Axiality. *Chem. Commun.* **2018**, *54* (30), 3685−3696.
(16) Thomas-Hargreaves, L. R.; Giansiracusa, M. J.; Gregson, M.; Zanda, E.; O'Donnell, F.; Wooles, A. J.; Chilton, N. F.; Liddle, S. T. Correlating Axial and Equatorial Ligand Field Effects to the Single-Molecule Magnet Performances of a Family of Dysprosium Bis-Methanediide Complexes. *Chem. Sci.* **2021**, *12* (11), 3911−3920.
(17) Canaj, A. B.; Singh, M. K.; Wilson, C.; Rajaraman, G.; Murrie, M. Chemical and in Silico Tuning of the Magnetisation Reversal Barrier in Pentagonal Bipyramidal Dy(III) Single-Ion Magnets. *Chem. Commun.* **2018**, *54* (59), 8273−8276.
(18) Le Roy, J. J.; Korobkov, I.; Murugesu, M. A Sandwich Complex with Axial Symmetry for Harnessing the Anisotropy in a Prolate Erbium(Iii) Ion. *Chem. Commun.* **2014**, *50* (13), 1602−1604.
(19) Zhang, P.; Zhang, L.; Wang, C.; Xue, S.; Lin, S.-Y.; Tang, J. Equatorially Coordinated Lanthanide Single Ion Magnets. *J. Am. Chem. Soc.* **2014**, *136* (12), 4484−4487.
(20) Goodwin, C. A. P.; Ortu, F.; Reta, D.; Chilton, N. F.; Mills, D. P. Molecular magnetic hysteresis at 60 kelvin in dysprosocenium. *Nature* **2017**, *548* (7668), 439−442.
(21) Guo, F.-S.; Day, B. M.; Chen, Y.-C.; Tong, M.-L.; Mansikkamäki, A.; Layfield, R. A. A Dysprosium Metallocene Single-Molecule Magnet Functioning at the Axial Limit. *Angew. Chem., Int. Ed.* **2017**, *56* (38), 11445−11449.
(22) Baniodeh, A.; Mondal, A.; Galeev, R.; Sukhanov, A.; Eremina, R.; Voronkova, V.; Anson, C. E.; Powell, A. K. How Far Can the Anisotropy Deviate from Uniaxiality in a Dy-Based Single-Molecule Magnet? Dinuclear Dy(III) Complex Study. *Appl. Magn. Reson.* **2017**, *48* (1), 101−113.
(23) Guo, F.-S.; Day, B. M.; Chen, Y.-C.; Tong, M.-L.; Mansikkamäki, A.; Layfield, R. A. Magnetic hysteresis up to 80 kelvin in a dysprosium metallocene single-molecule magnet. *Science* **2018**, *362* (6421), 1400−1403.
(24) Randall McClain, K.; Gould, C. A.; Chakarawet, K.; Teat, S. J.; Groshens, T. J.; Long, J. R.; Harvey, B. G. High-Temperature Magnetic Blocking and Magneto-Structural Correlations in a Series of Dysprosium(III) Metallocenium Single-Molecule Magnets. *Chem. Sci.* **2018**, *9* (45), 8492−8503.
(25) Moseley, D. H.; Stavretis, S. E.; Zhu, Z.; Guo, M.; Brown, C. M.; Ozerov, M.; Cheng, Y.; Daemen, L. L.; Richardson, R.; Knight, G.; Thirunavukkuarasu, K.; Ramirez-Cuesta, A. J.; Tang, J.; Xue, Z.-L. Inter-Kramers Transitions and Spin-Phonon Couplings in a Lanthanide-Based Single-Molecule Magnet. *Inorg. Chem.* **2020**, *59* (7), 5218−5230.
(26) Kragskow, J. G. C.; Marbey, J.; Buch, C. D.; Nehrkorn, J.; Ozerov, M.; Piligkos, S.; Hill, S.; Chilton, N. Analysis of vibronic coupling in a 4f molecular magnet with FIRMS. *Nat. Commun.* **2022**, *13*, 825.
(27) Bogani, L.; Wernsdorfer, W. Molecular Spintronics Using Single-Molecule Magnets. *Nat. Mater.* **2008**, *7* (3), 179−186.
(28) Atzori, M.; Sessoli, R. The Second Quantum Revolution: Role and Challenges of Molecular Chemistry. *J. Am. Chem. Soc.* **2019**, *141* (29), 11339−11352.
(29) Aravena, D.; Ruiz, E. Spin Dynamics in Single-Molecule Magnets and Molecular Qubits. *Dalton Trans.* **2020**, *49* (29), 9916−9928.
(30) Ruan, T.-T.; Moreno-Pineda, E.; Schulze, M.; Schlittenhardt, S.; Brietzke, T.; Holdt, H.-J.; Kuppusamy, S. K.; Wernsdorfer, W.; Ruben, M. Hilbert Space in Isotopologue Dy(III) SMM Dimers: Dipole Interaction Limit in [163/164Dy2(Tmhd)6(Tape)]0 Complexes. *Inorg. Chem.* **2023**, *62* (37), 15148−15156.
(31) Le Roy, J. J.; Ungur, L.; Korobkov, I.; Chibotaru, L. F.; Murugesu, M. Coupling Strategies to Enhance Single-Molecule Magnet Properties of Erbium-Cyclooctatetraenyl Complexes. *J. Am. Chem. Soc.* **2014**, *136* (22), 8003−8010.
(32) Chen, Y.-C.; Tong, M.-L. Single-Molecule Magnets beyond a Single Lanthanide Ion: The Art of Coupling. *Chem. Sci.* **2022**, *13*, 8716−8726.
(33) Gould, C. A.; McClain, K. R.; Reta, D.; Kragskow, J. G. C.; Marchiori, D. A.; Lachman, E.; Choi, E. S.; Analytis, J. G.; Britt, R. D.; Chilton, N. F.; Harvey, B. G.; Long, J. R. Ultrahard Magnetism

https://doi.org/10.1021/jacs.3c10412
J. Am. Chem. Soc. 2024, 146, 7243−7256

from Mixed-Valence Dilanthanide Complexes with Metal-Metal Bonding. *Science* **2022**, *375* (6577), 198−202.
(34) Demir, S.; Gonzalez, M. I.; Darago, L. E.; Evans, W. J.; Long, J. R. Giant Coercivity and High Magnetic Blocking Temperatures for N2 3- Radical-Bridged Dilanthanide Complexes upon Ligand Dissociation. *Nat. Commun.* **2017**, *8* (1), 2144.
(35) Zhang, P.; Benner, F.; Chilton, N. F.; Demir, S. Organometallic Lanthanide Bismuth Cluster Single-Molecule Magnets. *Chem.* **2022**, *8* (3), 717−730.
(36) Velkos, G.; Krylov, D. S.; Kirkpatrick, K.; Liu, X.; Spree, L.; Wolter, A. U. B.; Büchner, B.; Dorn, H. C.; Popov, A. A. Giant Exchange Coupling and Field-Induced Slow Relaxation of Magnetization in Gd 2 @C 79 N with a Single-Electron Gd-Gd Bond. *Chem. Commun.* **2018**, *54* (23), 2902−2905.
(37) Benner, F.; Demir, S. From Unprecedented 2,2′-Bisimidazole-Bridged Rare Earth Organometallics to Magnetic Hysteresis in the Dysprosium Congener. *Inorg. Chem. Front.* **2023**, *10*, 4981−4992.
(38) Benner, F.; La Droitte, L.; Cador, O.; Le Guennic, B.; Demir, S. Magnetic Hysteresis and Large Coercivity in Bisbenzimidazole Radical-Bridged Dilanthanide Complexes. *Chem. Sci.* **2023**, *14* (21), 5577−5592.
(39) Zhang, P.; Nabi, R.; Staab, J. K.; Chilton, N. F.; Demir, S. Taming Super-Reduced Bi23- Radicals with Rare Earth Cations. *J. Am. Chem. Soc.* **2023**, *145* (16), 9152−9163.
(40) Smith, J. A.; Galán-Mascarós, J. R.; Clérac, R.; Sun, J.-S.; Ouyang, X.; Dunbar, K. R. New Approaches to Magnetic Clusters with Hexacyanometallate Building Blocks. *Polyhedron* **2001**, *20* (11−14), 1727−1734.
(41) Le Roy, J. J.; Jeletic, M.; Gorelsky, S. I.; Korobkov, I.; Ungur, L.; Chibotaru, L. F.; Murugesu, M. An Organometallic Building Block Approach To Produce a Multidecker 4f Single-Molecule Magnet. *J. Am. Chem. Soc.* **2013**, *135* (9), 3502−3510.
(42) Pedersen, K. S.; Bendix, J.; Clérac, R. Single-Molecule Magnet Engineering: Building-Block Approaches. *Chem. Commun.* **2014**, *50* (34), 4396−4415.
(43) Harriman, K. L. M.; Murugesu, M. An Organolanthanide Building Block Approach to Single-Molecule Magnets. *Acc. Chem. Res.* **2016**, *49* (6), 1158−1167.
(44) Liu, Y.; Chen, Y.-C.; Liu, J.; Chen, W.-B.; Huang, G.-Z.; Wu, S.-G.; Wang, J.; Liu, J.-L.; Tong, M.-L. Cyanometallate-Bridged Didysprosium Single-Molecule Magnets Constructed with Single-Ion Magnet Building Block. *Inorg. Chem.* **2020**, *59* (1), 687−694.
(45) Ishikawa, N.; Iino, T.; Kaizu, Y. Interaction between F-Electronic Systems in Dinuclear Lanthanide Complexes with Phthalocyanines. *J. Am. Chem. Soc.* **2002**, *124* (38), 11440−11447.
(46) Ishikawa, N.; Iino, T.; Kaizu, Y. Determination of Ligand-Field Parameters and f-Electronic Structures of Hetero-Dinuclear Phthalocyanine Complexes with a Diamagnetic Yttrium(III) and a Paramagnetic Trivalent Lanthanide Ion. *J. Phys. Chem. A* **2002**, *106* (41), 9543−9550.
(47) Ishikawa, N.; Iino, T.; Kaizu, Y. Study of 1H NMR Spectra of Dinuclear Complexes of Heavy Lanthanides with Phthalocyanines Based on Separation of the Effects of Two Paramagnetic Centers. *J. Phys. Chem. A* **2003**, *107* (39), 7879−7884.
(48) Luttinger, J. M.; Tisza, L. Theory of Dipole Interaction in Crystals. *Phys. Rev.* **1946**, *70* (11−12), 954−964.
(49) Czech, R.; Villain, J. Instability of Two-Dimensional Ising Ferromagnets with Dipole Interactions. *J. Phys.: Condens. Matter* **1989**, *1* (3), 619−627.
(50) Vedmedenko, E. Y.; Ghazali, A.; Lévy, J.-C. S. Magnetic Structures of Ising and Vector Spins Monolayers by Monte-Carlo Simulations. *Surf. Sci.* **1998**, *402*−*404*, 391−395.
(51) Johnston, D. C. Magnetic Dipole Interactions in Crystals. *Phys. Rev. B* **2016**, *93* (1), 014421.
(52) Babkevich, P.; Jeong, M.; Matsumoto, Y.; Kovacevic, I.; Finco, A.; Toft-Petersen, R.; Ritter, C.; Månsson, M.; Nakatsuji, S.; Rønnow, H. Dimensional Reduction in Quantum Dipolar Antiferromagnets. *Phys. Rev. Lett.* **2016**, *116* (19), 197202.
(53) Ciftja, O. Exact Ground State Energy of a System with an Arbitrary Number of Dipoles at the Sites of a Regular One-Dimensional Crystal Lattice. *J. Phys. Chem. Solid.* **2023**, *172*, 111044.
(54) Batle, J. Minimum Energy Configurations for Interacting Dipoles in Simple Hypercubic Lattices. *Results Phys.* **2020**, *16*, 103114.
(55) Geldart, D. J. W.; Hargraves, P.; Fujiki, N. M.; Dunlap, R. A. Anisotropy of the Critical Magnetic Susceptibility of Gadolinium. *Phys. Rev. Lett.* **1989**, *62* (23), 2728−2731.
(56) Rotter, M.; Loewenhaupt, M.; Doerr, M.; Lindbaum, A.; Sassik, H.; Ziebeck, K.; Beuneu, B. Dipole Interaction and Magnetic Anisotropy in Gadolinium Compounds. *Phys. Rev. B* **2003**, *68* (14), 144418.
(57) Babkevich, P.; Finco, A.; Jeong, M.; Dalla Piazza, B.; Kovacevic, I.; Klughertz, G.; Krämer, K. W.; Kraemer, C.; Adroja, D. T.; Goremychkin, E.; Unruh, T.; Strässle, T.; Di Lieto, A.; Jensen, J.; Rønnow, H. M. Neutron Spectroscopic Study of Crystal-Field Excitations and the Effect of the Crystal Field on Dipolar Magnetism in LiRF4 (R = Gd, Ho, Er, Tm, and Yb). *Phys. Rev. B* **2015**, *92* (14), 144422.
(58) Hayashida, S.; Ishikawa, H.; Okamoto, Y.; Okubo, T.; Hiroi, Z.; Avdeev, M.; Manuel, P.; Hagihala, M.; Soda, M.; Masuda, T. Magnetic State Selected by Magnetic Dipole Interaction in the Kagome Antiferromagnet NaBa2Mn3F11. *Phys. Rev. B* **2018**, *97* (5), 054411.
(59) Ashhab, S.; Carignano, M.; Madjet, M. E. Order in the Ground State of a Simple Cubic Dipole Lattice in an External Field. *Int. J. Quantum Chem.* **2020**, *120* (1), No. e26053.
(60) Zinnatullin, A. L.; Cherosov, M. A.; Nosov, I. Yu.; Kiiamov, A. G.; Yusupov, R. V.; Vagizov, F. G. Magnetic Dipolar Correlations in Sillenite-Structure Bismuth Ferrite: Magnetic and Mössbauer Effect Studies. *J. Phys. Chem. Solid* **2022**, *164*, 110632.
(61) Lee, J.; Tatsuta, M.; Xu, A.; Bauch, E.; Ku, M. J. H.; Walsworth, R. L. Dressed-State Control of Effective Dipolar Interaction between Strongly-Coupled Solid-State Spins. *npj Quantum Inf.* **2023**, *9* (1), 77.
(62) Wernsdorfer, W.; Aliaga-Alcalde, N.; Hendrickson, D. N.; Christou, G. Exchange-Biased Quantum Tunnelling in a Supramolecular Dimer of Single-Molecule Magnets. *Nature* **2002**, *416* (6879), 406−409.
(63) Ishikawa, N.; Otsuka, S.; Kaizu, Y. The Effect of the f-f Interaction on the Dynamic Magnetism of a Coupled 4f8 System in a Dinuclear Terbium Complex with Phthalocyanines. *Angew. Chem., Int. Ed.* **2005**, *44* (5), 731−733.
(64) Lin, P.-H.; Burchell, T. J.; Ungur, L.; Chibotaru, L. F.; Wernsdorfer, W.; Murugesu, M. A Polynuclear Lanthanide Single-Molecule Magnet with a Record Anisotropic Barrier. *Angew. Chem.* **2009**, *121* (50), 9653−9656.
(65) Ke, H.; Gamez, P.; Zhao, L.; Xu, G.-F.; Xue, S.; Tang, J. Magnetic Properties of Dysprosium Cubanes Dictated by the M-O-M Angles of the [Dy4(M3-OH)4] Core. *Inorg. Chem.* **2010**, *49* (16), 7549−7557.
(66) Long, J.; Habib, F.; Lin, P.-H.; Korobkov, I.; Enright, G.; Ungur, L.; Wernsdorfer, W.; Chibotaru, L. F.; Murugesu, M. Single-Molecule Magnet Behavior for an Antiferromagnetically Superexchange-Coupled Dinuclear Dysprosium(III) Complex. *J. Am. Chem. Soc.* **2011**, *133* (14), 5319−5328.
(67) Guo, Y.-N.; Xu, G.-F.; Wernsdorfer, W.; Ungur, L.; Guo, Y.; Tang, J.; Zhang, H.-J.; Chibotaru, L. F.; Powell, A. K. Strong Axiality and Ising Exchange Interaction Suppress Zero-Field Tunneling of Magnetization of an Asymmetric Dy2 Single-Molecule Magnet. *J. Am. Chem. Soc.* **2011**, *133* (31), 11948−11951.
(68) Blagg, R. J.; Ungur, L.; Tuna, F.; Speak, J.; Comar, P.; Collison, D.; Wernsdorfer, W.; McInnes, E. J. L.; Chibotaru, L. F.; Winpenny, R. E. P. Magnetic Relaxation Pathways in Lanthanide Single-Molecule Magnets. *Nat. Chem.* **2013**, *5* (8), 673−678.
(69) Alexandropoulos, D. I.; Alaimo, A. A.; Sun, D.; Stamatatos, T. C. A New {Dy5} Single-Molecule Magnet Bearing the Schiff Base

https://doi.org/10.1021/jacs.3c10412
J. Am. Chem. Soc. 2024, 146, 7243−7256

Ligand N-Naphthalidene-2-Amino-5-Chlorophenol. *Magnetochemistry* **2018**, *4* (4), 48.
(70) Lu, G.; Liu, Y.; Deng, W.; Huang, G.-Z.; Chen, Y.-C.; Liu, J.-L.; Ni, Z.-P.; Giansiracusa, M.; Chilton, N. F.; Tong, M.-L. A Perfect Triangular Dysprosium Single-Molecule Magnet with Virtually Antiparallel Ising-like Anisotropy. *Inorg. Chem. Front.* **2020**, *7* (16), 2941−2948.
(71) Bode, B. E.; Fusco, E.; Nixon, R.; Buch, C. D.; Weihe, H.; Piligkos, S. Dipolar-Coupled Entangled Molecular 4f Qubits. *J. Am. Chem. Soc.* **2023**, *145* (5), 2877−2883.
(72) Habib, F.; Lin, P.-H.; Long, J.; Korobkov, I.; Wernsdorfer, W.; Murugesu, M. The Use of Magnetic Dilution To Elucidate the Slow Magnetic Relaxation Effects of a Dy2 Single-Molecule Magnet. *J. Am. Chem. Soc.* **2011**, *133* (23), 8830−8833.
(73) Moreno Pineda, E.; Chilton, N. F.; Marx, R.; Dörfel, M.; Sells, D. O.; Neugebauer, P.; Jiang, S.-D.; Collison, D.; van Slageren, J.; McInnes, E. J. L.; Winpenny, R. E. P. Direct measurement of dysprosium(III)dysprosium(III) interactions in a single-molecule magnet. *Nat. Commun.* **2014**, *5* (1), 5243.
(74) Giansiracusa, M. J.; Moreno-Pineda, E.; Hussain, R.; Marx, R.; Martínez Prada, M.; Neugebauer, P.; Al-Badran, S.; Collison, D.; Tuna, F.; van Slageren, J.; Carretta, S.; Guidi, T.; McInnes, E. J. L.; Winpenny, R. E. P.; Chilton, N. F. Measurement of Magnetic Exchange in Asymmetric Lanthanide Dimetallics: Toward a Transferable Theoretical Framework. *J. Am. Chem. Soc.* **2018**, *140* (7), 2504−2513.
(75) Orlova, A. P.; Hilgar, J. D.; Bernbeck, M. G.; Gembicky, M.; Rinehart, J. D. Intuitive Control of Low-Energy Magnetic Excitations via Directed Dipolar Interactions in a Series of Er(III)-Based Complexes. *J. Am. Chem. Soc.* **2022**, *144* (25), 11316−11325.
(76) Mandel, A.; Magull, J. Neue Benzylkomplexe Der Lanthanoiden. Darstellung Und Kristallstrukturen von [(C5Me5)2Y (CH2C6H5)(Thf)], [(C5Me5)2Sm(CH2C6H5)2K-(Thf)2]∞ Und [(C5Me5)Gd(CH2C6H5)2(Thf)]. *Z. Anorg. Allg. Chem.* **1996**, *622* (11), 1913−1919.
(77) Mandel, A.; Magull, J. Reaktionen von Lanthanoidhalogeniden Mit Alkalibenzylverbindungen. Darstellung Und Kristallstrukturen von [(Tmeda)(C6H5CH2)2Y(μ-Br)2Li(Tmeda)], [(Tmeda)-2SmBr(μ-Br)2Li(Tmeda)] Und [(Dme)2SmBr(μ-Br)]2. *Z. Anorg. Allg. Chem.* **1997**, *623* (10), 1542−1546.
(78) Bambirra, S.; Brandsma, M. J. R.; Brussee, E. A. C.; Meetsma, A.; Hessen, B.; Teuben, J. H. Yttrium Alkyl and Benzyl Complexes with Amino-Amidinate Monoanionic Ancillary Ligands. *Organometallics* **2000**, *19* (16), 3197−3204.
(79) Avent, A. G.; Cloke, F. G. N.; Elvidge, B. R.; Hitchcock, P. B. Yttrium Complexes Incorporating the Chelating Diamides {ArN-(CH2)xNAr}2- (Ar = C6H3−2,6-iPr2, x = 2, 3) and Their Unusual Reaction with Phenylsilane. *Dalton Trans.* **2004**, No. 7, 1083−1096.
(80) Mills, D. P.; Cooper, O. J.; McMaster, J.; Lewis, W.; Liddle, S. T. Synthesis and Reactivity of the Yttrium-Alkyl-Carbene Complex [Y(BIPM)(CH2C6H5)(THF)] (BIPM = {C(PPh2NSiMe3)2}). *Dalton Trans.* **2009**, No. 23, 4547−4555.
(81) Kenward, A. L.; Piers, W. E.; Parvez, M. Low-Coordinate Organoyttrium Complexes Supported by β-Diketiminato Ligands. *Organometallics* **2009**, *28* (10), 3012−3020.
(82) Ge, S.; Meetsma, A.; Hessen, B. Scandium, Yttrium, and Lanthanum Benzyl and Alkynyl Complexes with the N-(2-Pyrrolidin-1-Ylethyl)-1,4-Diazepan-6-Amido Ligand: Synthesis, Characterization, and Z-Selective Catalytic Linear Dimerization of Phenylacetylenes. *Organometallics* **2009**, *28* (3), 719−726.
(83) Döring, C.; Kretschmer, W. P.; Kempe, R. Aminopyridinate-Stabilized Lanthanoid Complexes: Synthesis, Structure and Polymerization of Ethylene and Isoprene. *Eur. J. Inorg. Chem.* **2010**, *2010* (18), 2853−2860.
(84) Evans, L. T. J.; Coles, M. P.; Cloke, F. G. N.; Hitchcock, P. B. Group 3 Complexes Incorporating (Furyl)-Substituted Disilazide Ligands. *Inorg. Chim. Acta* **2010**, *363* (6), 1114−1125.
(85) Wooles, A. J.; Mills, D. P.; Lewis, W.; Blake, A. J.; Liddle, S. T. Lanthanide Tri-Benzyl Complexes: Structural Variations and Useful Precursors to Phosphorus-Stabilised Lanthanide Carbenes. *Dalton Trans.* **2010**, *39* (2), 500−510.
(86) Yi, W.; Zhang, J.; Zhang, F.; Zhang, Y.; Chen, Z.; Zhou, X. Versatile Reactivity of Scorpionate-Anchored Yttrium-Dialkyl Complexes towards Unsaturated Substrates. *Chem.—Eur. J.* **2013**, *19* (36), 11975−11983.
(87) Yi, W.; Huang, S.; Zhang, J.; Chen, Z.; Zhou, X. Reactivity of Scorpionate-Anchored Yttrium Alkyl Primary Amido Complexes toward Carbodiimides. Insertion Selectivity of Y-NHAr and Y-CH2Ph Bonds. *Organometallics* **2013**, *32* (19), 5409−5415.
(88) Huang, W.; Upton, B. M.; Khan, S. I.; Diaconescu, P. L. Synthesis and Characterization of Paramagnetic Lanthanide Benzyl Complexes. *Organometallics* **2013**, *32* (5), 1379−1386.
(89) Mills, D. P.; Soutar, L.; Cooper, O. J.; Lewis, W.; Blake, A. J.; Liddle, S. T. Reactivity of the Yttrium Alkyl Carbene Complex [Y(BIPM)(CH2C6H5)(THF)] (BIPM = {C(PPh2NSiMe3)2})2-: From Insertions, Substitutions, and Additions to Nontypical Transformations. *Organometallics* **2013**, *32* (5), 1251−1264.
(90) Zhang, F.; Zhang, J.; Zhang, Y.; Hong, J.; Zhou, X. Rare-Earth-Metal-Catalyzed Addition of Terminal Monoalkynes and Dialkynes with Aryl-Substituted Symmetrical or Unsymmetrical Carbodiimides. *Organometallics* **2014**, *33* (21), 6186−6192.
(91) Brosmer, J. L.; Diaconescu, P. L. Yttrium-Alkyl Complexes Supported by a Ferrocene-Based Phosphinimine Ligand. *Organometallics* **2015**, *34* (11), 2567−2572.
(92) Wang, X.; Brosmer, J. L.; Thevenon, A.; Diaconescu, P. L. Highly Active Yttrium Catalysts for the Ring-Opening Polymerization of ε-Caprolactone and δ-Valerolactone. *Organometallics* **2015**, *34* (19), 4700−4706.
(93) Thim, R.; Dietrich, H. M.; Bonath, M.; Maichle-Mössmer, C.; Anwander, R. Pentamethylcyclopentadienyl-Supported Rare-Earth-Metal Benzyl, Amide, and Imide Complexes. *Organometallics* **2018**, *37* (16), 2769−2777.
(94) Evans, W. J.; Ulibarri, T. A.; Ziller, J. W. Reactivity of Samarium Complex [(C5Me5)2Sm(.Mu.-H)]2 in Ether and Arene Solvents. X-Ray Crystal Structures of the Internally Metalated Complex (C5Me5)2Sm(.Mu.-H)(.Mu.-CH2C5Me4)Sm(C5Me5), the Benzyl Complex (C5Me5)2Sm(CH2C6H5)(THF), and the Siloxide Complex [(C5Me5)2Sm(THF)]2(.Mu.-OSiMe2OSi-Me2O). *Organometallics* **1991**, *10* (1), 134−142.
(95) Bambirra, S.; Meetsma, A.; Bart Hessen, B. Tris(4-methylbenzyl)(1,4,7-trimethyl-1,4,7-triazacyclononane)lanthanum-(III). *Acta Crystallogr. Sec. E* **2007**, *63* (12), m2891.
(96) Bambirra, S.; Perazzolo, F.; Boot, S. J.; Sciarone, T. J. J.; Meetsma, A.; Hessen, B. Strategies for the Synthesis of Lanthanum Dialkyl Complexes with Monoanionic Ancillary Ligands. *Organometallics* **2008**, *27* (4), 704−712.
(97) Meyer, N.; Roesky, P. W. Synthesis and Characterization of an Enantiomerically Pure Lutetium Benzyl Complex. *Z. Anorg. Allg. Chem.* **2008**, *634* (12−13), 2171−2174.
(98) Meyer, N.; Roesky, P. W.; Bambirra, S.; Meetsma, A.; Hessen, B.; Saliu, K.; Takats, J. Synthesis and Structures of Scandium and Lutetium Benzyl Complexes. *Organometallics* **2008**, *27* (7), 1501−1505.
(99) Wong, A. W.; Miller, K. L.; Diaconescu, P. L. Reactions of Aromatic N-Heterocycles with a Lutetium Benzyl Complex Supported by a Ferrocene-Diamide Ligand. *Dalton Trans.* **2010**, *39* (29), 6726−6731.
(100) Trambitas, A. G.; Panda, T. K.; Jenter, J.; Roesky, P. W.; Daniliuc, C.; Hrib, C. G.; Jones, P. G.; Tamm, M. Rare-Earth Metal Alkyl, Amido, and Cyclopentadienyl Complexes Supported by Imidazolin-2-Iminato Ligands: Synthesis, Structural Characterization, and Catalytic Application. *Inorg. Chem.* **2010**, *49* (5), 2435−2446.
(101) Zhang, X.; Wang, C.; Xue, M.; Zhang, Y.; Yao, Y.; Shen, Q. Synthesis and Structure of Samarium Benzyl Complex Supported by Bridged Bis(Guanidinate) Ligand and Its Reactivity toward Nitriles and Phenyl Isocyanate. *J. Organomet. Chem.* **2012**, *716*, 86−94.
(102) Lampland, N. L.; Zhu, J.; Hovey, M.; Jana, B.; Ellern, A.; Sadow, A. D. Piano-Stool Lutetium Amido and Imido Compounds

https://doi.org/10.1021/jacs.3c10412
J. Am. Chem. Soc. 2024, 146, 7243−7256

Supported by a Constrained Bis(Oxazoline)Cyclopentadienyl Ligand. *Inorg. Chem.* **2015**, *54* (14), 6938−6946.
(103) Rachor, S. G.; Cleaves, P. A.; Robertson, S. D.; Mansell, S. M. NMR Spectroscopic Study of the Adduct Formation and Reactivity of Homoleptic Rare Earth Amides with Alkali Metal Benzyl Compounds, and the Crystal Structures of [Li(TMEDA)2][Nd{N(SiMe3)2}3(CH2Ph)] and [{Li(TMP)}2{Li(Ph)}]2. *J. Organomet. Chem.* **2018**, *857*, 101−109.
(104) Demkin, A. G.; Savkov, B. Yu.; Sukhikh, T. S.; Konchenko, S. N. Synthesis and structure of a new neodymium complex with an unusual type of coordination of the benzyl ligand. *J. Struct. Chem.* **2021**, *62* (1), 116−122.
(105) Shi, X.; Deng, P.; Rajeshkumar, T.; Zhao, L.; Maron, L.; Cheng, J. A Mononuclear Divalent Ytterbium Hydrido Complex Supported by a Super-Bulky Scorpionate Ligand. *Chem. Commun.* **2021**, *57* (78), 10047−10050.
(106) Harder, S. Syntheses and Structures of Homoleptic Lanthanide Complexes with Chelating O-Dimethylaminobenzyl Ligands: Key Precursors in Lanthanide Chemistry. *Organometallics* **2005**, *24* (3), 373−379.
(107) Bambirra, S.; Meetsma, A.; Hessen, B. Lanthanum Tribenzyl Complexes as Convenient Starting Materials for Organolanthanum Chemistry. *Organometallics* **2006**, *25* (14), 3454−3462.
(108) Ge, S.; Meetsma, A.; Hessen, B. Neutral and Cationic Rare Earth Metal Alkyl and Benzyl Compounds with the 1,4,6-Trimethyl-6-Pyrrolidin-1-Yl-1,4-Diazepane Ligand and Their Performance in the Catalytic Hydroamination/Cyclization of Aminoalkenes. *Organometallics* **2008**, *27* (20), 5339−5346.
(109) Mills, D. P.; Wooles, A. J.; McMaster, J.; Lewis, W.; Blake, A. J.; Liddle, S. T. Heteroleptic [M(CH2C6H5)2(I)(THF)3] Complexes (M = Y or Er): Remarkably Stable Precursors to Yttrium and Erbium T-Shaped Carbenes. *Organometallics* **2009**, *28* (23), 6771−6776.
(110) Lin, D.; Chen, J.; Luo, C.; Zhang, Y.; Yao, Y.; Luo, Y. Rare Earth Metal Benzyl Complexes Bearing Bridged-Indenyl Ligand for Highly Active Polymerization of Methyl Methacrylate. *J. Organomet. Chem.* **2009**, *694* (18), 2976−2980.
(111) Werkema, E. L.; Andersen, R. A.; Maron, L.; Eisenstein, O. The Reaction of Bis(1,2,4-Tri-t-Butylcyclopentadienyl)-Ceriumbenzyl, Cp′2CeCH2Ph, with Methylhalides: A Metathesis Reaction That Does Not Proceed by a Metathesis Transition State. *Dalton Trans.* **2010**, *39* (29), 6648−6660.
(112) Zhang, Z.; Zhang, L.; Li, Y.; Hong, L.; Chen, Z.; Zhou, X. Activation of Bis(Guanidinate)Lanthanide Alkyl and Aryl Complexes on Elemental Sulfur: Synthesis and Characterization of Bis-(Guanidinate)Lanthanide Thiolates and Disulfides. *Inorg. Chem.* **2010**, *49* (12), 5715−5722.
(113) Diaconescu, P. L. Reactions of Aromatic N-Heterocycles with d^0f^n-Metal Alkyl Complexes Supported by Chelating Diamide Ligands. *Acc. Chem. Res.* **2010**, *43* (10), 1352−1363.
(114) Liu, B.; Sun, G.; Li, S.; Liu, D.; Cui, D. Isoprene Polymerization with Iminophosphonamide Rare-Earth-Metal Alkyl Complexes: Influence of Metal Size on the Regio- and Stereoselectivity. *Organometallics* **2015**, *34* (16), 4063−4068.
(115) Gregson, M.; Chilton, N. F.; Ariciu, A.-M.; Tuna, F.; Crowe, I. F.; Lewis, W.; Blake, A. J.; Collison, D.; McInnes, E. J. L.; Winpenny, R. E. P.; Liddle, S. T. A Monometallic Lanthanide Bis(Methanediide) Single Molecule Magnet with a Large Energy Barrier and Complex Spin Relaxation Behaviour. *Chem. Sci.* **2016**, *7* (1), 155−165.
(116) Wolf, B. M.; Stuhl, C.; Anwander, R. Synthesis of Homometallic Divalent Lanthanide Organoimides from Benzyl Complexes. *Chem. Commun.* **2018**, *54* (64), 8826−8829.
(117) Birkelbach, V. M.; Thim, R.; Stuhl, C.; Maichle-Mössmer, C.; Anwander, R. Potential Precursors for Terminal Methylidene Rare-Earth-Metal Complexes Supported by a Superbulky Tris-(Pyrazolyl)Borato Ligand. *Chem.—Eur. J.* **2019**, *25* (64), 14711−14720.
(118) Wang, Y.; Del Rosal, I.; Qin, G.; Zhao, L.; Maron, L.; Shi, X.; Cheng, J. Scandium and Lanthanum Hydride Complexes Stabilized by Super-Bulky Penta-Arylcyclopentadienyl Ligands. *Chem. Commun.* **2021**, *57* (63), 7766−7769.
(119) Hilgar, J. D.; Bernbeck, M. G.; Rinehart, J. D. Million-Fold Relaxation Time Enhancement across a Series of Phosphino-Supported Erbium Single-Molecule Magnets. *J. Am. Chem. Soc.* **2019**, *141* (5), 1913−1917.
(120) Bernbeck, M. G.; Hilgar, J. D.; Rinehart, J. D. Probing Axial Anisotropy in Dinuclear Alkoxide-Bridged Er-COT Single-Molecule Magnets. *Polyhedron* **2020**, *175*, 114206.
(121) Hodgson, K. O.; Raymond, K. N. Dimeric.Pi.-Cyclooctatetraene Dianion Complex of Cerium(III). Crystal and Molecular Structure of [Ce(C8H8)Cl.20C4H8]2. *Inorg. Chem.* **1972**, *11* (1), 171−175.
(122) Mashima, K.; Nakayama, Y.; Nakamura, A.; Kanehisa, N.; Kai, Y.; Takaya, H. A New Convenient Preparation of Monocyclooctatetraenyl-Lanthanide Complexes from Metallic Lanthanides and Oxidants. *J. Organomet. Chem.* **1994**, *473* (1−2), 85−91.
(123) Zhang, S.; Wei, G.; Chen, W.; Liu, J. Synthesis and crystal structure of {(C8H8)Dy[μ-OCH2(CH2)2CH═CH2(THF)}2. *Polyhedron* **1994**, *13* (12), 1927−1930.
(124) Cendrowski-Guillaume, S. M.; Nierlich, M.; Lance, M.; Ephritikhine, M. First Chemical Transformations of Lanthanide Borohydride Compounds: Synthesis and Crystal Structures of [(η-C8H8)Nd(BH4)(THF)]2 and [(η-C8H8)Nd(THF)4] [BPh4]. *Organometallics* **1998**, *17* (5), 786−788.
(125) Cendrowski-Guillaume, S. M.; Le Gland, G.; Nierlich, M.; Ephritikhine, M. Lanthanide Borohydrides as Precursors to Organometallic Compounds. Mono(Cyclooctatetraenyl) Neodymium Complexes. *Organometallics* **2000**, *19* (26), 5654−5660.
(126) Visseaux, M.; Nief, F.; Ricard, L. Synthesis of Mixed Phospholyl/Cyclooctatetraenyl-Lanthanide Complexes. Crystal and Molecular Structure of (Cyclooctatetraenyl)[3,4-Dimethyl-2,5-Bis-(Trimethylsilyl)-Phospholyl](Tetrahydrofuran)Neodymium. *J. Organomet. Chem.* **2002**, *647* (1−2), 139−144.
(127) Evans, W. J.; Champagne, T. M.; Davis, B. L.; Allen, N. T.; Nyce, G. W.; Johnston, M. A.; Lin, Y.-C.; Khvostov, A.; Ziller, J. W. Structural Studies of Mono(Pentamethylcyclopentadienyl)-Lanthanide Complexes. *J. Coord. Chem.* **2006**, *59* (10), 1069−1087.
(128) Meermann, C.; Ohno, K.; Törnroos, K. W.; Mashima, K.; Anwander, R. Rare-Earth Metal Bis(Dimethylsilyl)Amide Complexes Supported by Cyclooctatetraenyl Ligands. *Eur. J. Inorg. Chem.* **2009**, *2009* (1), 76−85.
(129) Edelmann, A.; Lorenz, V.; Hrib, C. G.; Hilfert, L.; Blaurock, S.; Edelmann, F. T. Steric Effects in Lanthanide Sandwich Complexes Containing Bulky Cyclooctatetraenyl Ligands. *Organometallics* **2013**, *32* (5), 1435−1444.
(130) Hilgar, J. D.; Flores, B. S.; Rinehart, J. D. Ferromagnetic Coupling in a Chloride-Bridged Erbium Single-Molecule Magnet. *Chem. Commun.* **2017**, *53* (53), 7322−7324.
(131) Hong, J.; Li, Z.; Chen, Z.; Weng, L.; Zhou, X.; Zhang, L. Small Molecule Activation by Mixed Methyl/Methylidene Rare Earth Metal Complexes. *Dalton Trans.* **2016**, *45* (15), 6641−6649.
(132) Raeder, J.; Reiners, M.; Baumgarten, R.; Münster, K.; Baabe, D.; Freytag, M.; Jones, P. G.; Walter, M. D. Synthesis and Molecular Structure of Pentadienyl Complexes of the Rare-Earth Metals. *Dalton Trans.* **2018**, *47* (41), 14468−14482.
(133) Fdez Galván, I.; Vacher, M.; Alavi, A.; Angeli, C.; Aquilante, F.; Autschbach, J.; Bao, J. J.; Bokarev, S. I.; Bogdanov, N. A.; Carlson, R. K.; Chibotaru, L. F.; Creutzberg, J.; Dattani, N.; Delcey, M. G.; Dong, S. S.; Dreuw, A.; Freitag, L.; Frutos, L. M.; Gagliardi, L.; Gendron, F.; Giussani, A.; González, L.; Grell, G.; Guo, M.; Hoyer, C. E.; Johansson, M.; Keller, S.; Knecht, S.; Kovačević, G.; Källman, E.; Li Manni, G.; Lundberg, M.; Ma, Y.; Mai, S.; Malhado, J. P.; Malmqvist, P. Å.; Marquetand, P.; Mewes, S. A.; Norell, J.; Olivucci, M.; Oppel, M.; Phung, Q. M.; Pierloot, K.; Plasser, F.; Reiher, M.; Sand, A. M.; Schapiro, I.; Sharma, P.; Stein, C. J.; Sørensen, L. K.; Truhlar, D. G.; Ugandi, M.; Ungur, L.; Valentini,

https://doi.org/10.1021/jacs.3c10412
J. Am. Chem. Soc. 2024, 146, 7243−7256

A.; Vancoillie, S.; Veryazov, V.; Weser, O.; Wesołowski, T. A.; Widmark, P.-O.; Wouters, S.; Zech, A.; Zobel, J. P.; Lindh, R. OpenMolcas: From Source Code to Insight. *J. Chem. Theory Comput.* **2019**, *15* (11), 5925−5964.
(134) von Ragué Schleyer, P.; Kos, A. J.; Wilhelm, D.; Clark, T.; Boche, G.; Decher, G.; Etzrodt, H.; Dietrich, H.; Mahdi, W. The Influence of Carbanion Orbital Orientation and Charge Distribution on the Structures of Polylithium Compounds. *J. Chem. Soc., Chem. Commun.* **1984**, No. 22, 1495−1496.
(135) Binkowska, I.; Koput, J.; Jarczewski, A. Computational and Experimental Study of Charge Distribution in the α-Disulfonyl Carbanions. *J. Mol. Struct.* **2014**, *1062*, 35−43.
(136) Alabugin, I. V.; Bresch, S.; Manoharan, M. Hybridization Trends for Main Group Elements and Expanding the Bent's Rule Beyond Carbon: More than Electronegativity. *J. Phys. Chem. A* **2014**, *118* (20), 3663−3677.
(137) Nguyen, L. H.; Pham-Tran, N.-N. Validation of Valence Bond and Molecular Orbital Models in Analyzing the Anionic Hyperconjugation Effect on the Stability of Alkyl and Fluorinated Carbanions in Gaseous Phase. *J. Phys. Org. Chem.* **2023**, *36* (6), No. e4490.
(138) Neese, F. The ORCA Program System. *Wiley Interdiscip. Rev. Comput. Mol. Sci.* **2012**, *2* (1), 73−78.
(139) Neese, F. Software Update: The ORCA Program System, Version 4.0. *Wiley Interdiscip. Rev. Comput. Mol. Sci.* **2018**, *8* (1), No. e1327.
(140) Meng, Y.-S.; Yang, M.-W.; Xu, L.; Xiong, J.; Hu, J.-Y.; Liu, T.; Wang, B.-W.; Gao, S. Design Principle of Half-Sandwich Type Erbium Single-Ion Magnets through Crystal Field Engineering: A Combined Magnetic and Electronic Structure Study. *Dalton Trans.* **2019**, *48* (28), 10407−10411.
(141) Chibotaru, L. F.; Ungur, L.; Soncini, A. The Origin of Nonmagnetic Kramers Doublets in the Ground State of Dysprosium Triangles: Evidence for a Toroidal Magnetic Moment. *Angew. Chem., Int. Ed.* **2008**, *47* (22), 4126−4129.
(142) Chibotaru, L. F.; Ungur, L.; Aronica, C.; Elmoll, H.; Pilet, G.; Luneau, D. Structure, Magnetism, and Theoretical Study of a Mixed-Valence CoII3CoIII4 Heptanuclear Wheel: Lack of SMM Behavior despite Negative Magnetic Anisotropy. *J. Am. Chem. Soc.* **2008**, *130* (37), 12445−12455.
(143) Ungur, L.; Van den Heuvel, W.; Chibotaru, L. F. Ab Initio Investigation of the Non-Collinear Magnetic Structure and the Lowest Magnetic Excitations in Dysprosium Triangles. *New J. Chem.* **2009**, *33* (6), 1224−1230.
(144) Ungur, L.; Chibotaru, L. F. Magnetic Anisotropy in the Excited States of Low Symmetry Lanthanide Complexes. *Phys. Chem. Chem. Phys.* **2011**, *13* (45), 20086−20090.
(145) Lunghi, A. Spin-Phonon Relaxation in Magnetic Molecules: Theory, Predictions and Insights. In *Computational Modelling of Molecular Nanomagnets*; Rajaraman, G., Ed.; Springer International Publishing: Cham, 2023; pp 219−289.
(146) Haase, W. Oliver Kahn: Molecular Magnetism. VCH-Verlag, Weinheim, New York 1993. ISBN 3−527−89566−3, 380 Seiten, Preis: DM 154,—. *Ber. Bunsenges. Phys. Chem.* **1994**, *98* (9), 1208.
(147) Gatteschi, D.; Sessoli, R.; Villain, J. *Molecular Nanomagnets*; Oxford University Press, 2006; Vol. *376*.
(148) Orlova, A. P.; Varley, M. S.; Bernbeck, M. G.; Kirkpatrick, K. M.; Bunting, P. C.; Gembicky, M.; Rinehart, J. D. Molecular Network Approach to Anisotropic Ising Lattices: Parsing Magnetization Dynamics in Er3+ Systems with 0−3-Dimensional Spin Interactivity. *J. Am. Chem. Soc.* **2023**, *145* (40), 22265−22275.
(149) Sievers, A. J.; Tinkham, M. Far Infrared Spectra of Rare-Earth Iron Garnets. *Phys. Rev.* **1963**, *129* (5), 1995−2004.
(150) Bloor, D.; Copland, G. M. Far Infrared Spectra of Magnetic Ions in Crystals. *Rep. Prog. Phys.* **1972**, *35* (3), 1173−1264.
(151) Sirenko, A. A.; O'Malley, S. M.; Ahn, K. H.; Park, S.; Carr, G. L.; Cheong, S.-W. Infrared-Active Excitations Related to Ho 3 + Ligand-Field Splitting at the Commensurate-Incommensurate Magnetic Phase Transition in HoMn 2 O 5. *Phys. Rev. B* **2008**, *78* (17), 174405.
(152) Rogers, P. D.; Choi, Y. J.; Standard, E. C.; Kang, T. D.; Ahn, K. H.; Dubroka, A.; Marsik, P.; Wang, Ch.; Bernhard, C.; Park, S.; Cheong, S.-W.; Kotelyanskii, M.; Sirenko, A. A. Adjusted Oscillator Strength Matching for Hybrid Magnetic and Electric Excitations in Dy 3 Fe 5 O 12 Garnet. *Phys. Rev. B* **2011**, *83* (17), 174407.
(153) Albino, A.; Benci, S.; Tesi, L.; Atzori, M.; Torre, R.; Sanvito, S.; Sessoli, R.; Lunghi, A. First-Principles Investigation of Spin-Phonon Coupling in Vanadium-Based Molecular Spin Quantum Bits. *Inorg. Chem.* **2019**, *58* (15), 10260−10268.
(154) Blockmon, A. L.; Ullah, A.; Hughey, K. D.; Duan, Y.; O'Neal, K. R.; Ozerov, M.; Baldoví, J. J.; Aragó, J.; Gaita-Ariño, A.; Coronado, E.; Musfeldt, J. L. Spectroscopic Analysis of Vibronic Relaxation Pathways in Molecular Spin Qubit [Ho(W5O18)2]9-: Sparse Spectra Are Key. *Inorg. Chem.* **2021**, *60* (18), 14096−14104.
(155) Moseley, D. H.; Stavretis, S. E.; Thirunavukkuarasu, K.; Ozerov, M.; Cheng, Y.; Daemen, L. L.; Ludwig, J.; Lu, Z.; Smirnov, D.; Brown, C. M.; Pandey, A.; Ramirez-Cuesta, A. J.; Lamb, A. C.; Atanasov, M.; Bill, E.; Neese, F.; Xue, Z.-L. Spin-Phonon Couplings in Transition Metal Complexes with Slow Magnetic Relaxation. *Nat. Commun.* **2018**, *9* (1), 2572.
(156) Stavretis, S. E.; Moseley, D. H.; Fei, F.; Cui, H.-H.; Cheng, Y.; Podlesnyak, A. A.; Wang, X.; Daemen, L. L.; Hoffmann, C. M.; Ozerov, M.; Lu, Z.; Thirunavukkuarasu, K.; Smirnov, D.; Chang, T.; Chen, Y.-S.; Ramirez-Cuesta, A. J.; Chen, X.-T.; Xue, Z.-L. (B.). Spectroscopic Studies of the Magnetic Excitation and Spin-Phonon Couplings in a Single-Molecule Magnet. *Chem.—Eur. J.* **2019**, *25* (69), 15846−15857.
(157) Kragskow, J. G. C.; Marbey, J.; Buch, C. D.; Nehrkorn, J.; Ozerov, M.; Piligkos, S.; Hill, S.; Chilton, N. F. Analysis of Vibronic Coupling in a 4f Molecular Magnet with FIRMS. *Nat. Commun.* **2022**, *13* (1), 825.
(158) Blockmon, A. L.; Ullah, A.; Hughey, K. D.; Duan, Y.; O'Neal, K. R.; Ozerov, M.; Baldoví, J. J.; Aragó, J.; Gaita-Ariño, A.; Coronado, E.; Musfeldt, J. L. Spectroscopic Analysis of Vibronic Relaxation Pathways in Molecular Spin Qubit [Ho(W5O18)2]9-: Sparse Spectra Are Key. *Inorg. Chem.* **2021**, *60* (18), 14096−14104.
(159) Görller-Walrand, C.; Binnemans, K. Spectral Intensities of F-f Transitions. *Handbook on the Physics and Chemistry of Rare Earths*; Elsevier, 1998; Vol. *25*, pp 101−264, Chapter 167.
(160) Chen, Y.-C.; Liu, J.-L.; Ungur, L.; Liu, J.; Li, Q.-W.; Wang, L.-F.; Ni, Z.-P.; Chibotaru, L. F.; Chen, X.-M.; Tong, M.-L. Symmetry-Supported Magnetic Blocking at 20 K in Pentagonal Bipyramidal Dy(III) Single-Ion Magnets. *J. Am. Chem. Soc.* **2016**, *138* (8), 2829−2837.
(161) Lorenz, V.; Liebing, P.; Böhme, M.; Buchholz, A.; Plass, W.; Geue, N.; Hilfert, L.; Busse, S.; Engelhardt, F.; Hrib, C. G.; Edelmann, F. T. Lanthanide(III) Sandwich and Half-Sandwich Complexes with Bulky Cyclooctatetraenyl Ligands: Synthesis, Structures, and Magnetic Properties. *Eur. J. Inorg. Chem.* **2017**, *2017* (41), 4840−4849.
(162) Lorenz, V.; Schmiege, B. M.; Hrib, C. G.; Ziller, J. W.; Edelmann, A.; Blaurock, S.; Evans, W. J.; Edelmann, F. T. Unprecedented Bending and Rearrangement of F-Element Sandwich Complexes Induced by Superbulky Cyclooctatetraenide Ligands. *J. Am. Chem. Soc.* **2011**, *133* (5), 1257−1259.

https://doi.org/10.1021/jacs.3c10412
J. Am. Chem. Soc. 2024, 146, 7243−7256